MEASUREMENT AND ZERO-DELAY FINDING TECHNIQUES FOR ULTRASHORT OPTICAL PULSES USING LIGHT-EMITTING DIODES AS DETECTORS

By

ETHAN JOHN ABELE

Bachelor of Science in Electrical and Computer Engineering

Oklahoma State University

Stillwater, Oklahoma

2014

Submitted to the Faculty of the
Graduate College of the
Oklahoma State University
in partial fulfillment of
the requirements for
the Degree of
MASTER OF SCIENCE OR ARTS
December 2016

MEASUREMENT AND ZERO-DELAY FINDING TECHNIQUES FOR ULTRASHORT OPTICAL PULSES USING LIGHT-EMITTING DIODES AS DETECTORS

Thesis Approved:

Dr. Weili Zhang

Thesis Adviser

Dr. John O'Hara

Dr. Daniel Grischkowsky

Name: Ethan Abele

Date of Degree: DECEMBER, 2016

Title of Study: MEASUREMENT AND ZERO-DELAY FINDING TECHNIQUES FOR ULTRASHORT OPTICAL PULSES USING LIGHT-EMITTING DIODES AS DETECTORS

Major Field: Electrical and Computer Engineering

Abstract: The focus of this research was on the testing and characterization of light emitting diodes (LEDs) when used as replacements for second harmonic crystals in optical autocorrelation measurements. A range of experiments were performed to determine the response of these devices under various operating conditions. The results of these experiments were found to be inconsistent with the majority of previous work, producing inaccurately wide pulse width measurements. The measurements also show signal shoulders which are separate from the autocorrelation peak. These shoulders extend over a very long range (several picoseconds), and have useful applications for finding the point of zero delay in experimental setups. Theoretical analysis supported by simulation was also performed to provide insight into the mechanism at work to produce these features. While further investigation is required, this research has produced two very useful results. The inaccuracy which has been discovered in the pulse width measurements has provided a cause for caution when using LEDs in autocorrelation systems. More importantly, a new application has been identified for these measurements, and this application is improved by the features that make autocorrelation measurement undesirable.

TABLE OF CONTENTS

Chapter Page

I. INTRODUCTION 8

Motivation 8
Previous Work 9
Current Work 10
Outline 12

II. FOUNDATIONAL TECHNIQUE AND USE OF LEDS 14

Necessity of Nonlinear Response 14
Nonlinear Carrier Generation in LEDs 15
Use of Two-Photon Absorption for Autocorrelation Measurements 17
Comparison to Standard SHG Crystal Autocorrelators 18

III. SURVEY OF PREVIOUS RESULTS 20

Other Device Structures 21
Broadening and Other Factors 22
Summary 23

IV. EXPERIMENTAL RESULTS 24

Preparation of LEDs 24
Basic Autocorrelation Measurements 25
Amplitude Testing 32
Variable Beam Testing 34
Saturation Tests 42
Broadening Tests 45
Tests with Alternate LED 49
Discussion of Experiments 52

Chapter Page

V. THEORETICAL STUDIES....54

Eliminating Model Parameters....55
Basic Carrier Generation Model....57
Addition of Free Carrier Absorption Mechanism....62
Carrier Decay and Collection....67
Varying Pulse Width....73
Discussion of Simulations....74

VI. CONCLUSION....76

REFERENCES....78

APPENDICES....81

LIST OF FIGURES

Figure Page

Figure 1: Two-photon transition 9
Figure 2: Results of analytical autocorrelation solution 11
Figure 3: Intensity Profiles and Resulting Carrier Generation for (a) Large seperation, (b) Reduced seperation, (c) Partial overlap. Notice that the final resulting carrier density does not change until overlap occurs. 12
Figure 4: Through-hole style LED. (a) Unmodified construction (b) After grind and polish. 18
Figure 5: Intensity autocorrelator with BBO crystal 19
Figure 6: Intensity autocorrelator with LED 21
Figure 7: Initial raw autocorrelation measurements 22
Figure 8: Scaled autocorrelation traces 23
Figure 9: Wider scan of original measurements with amber LED 24
Figure 10: Autocorrelation signal dependence on average beam power 26
Figure 11: Autocorrelation with 20mW average power per beam 27
Figure 12: Varying beam 1 power with beam 2 power held at 40mw, both beams chopped. 28
Figure 13:Varying beam 2 power with beam 1 power held at 40mw, both beams chopped. 29
Figure 14: In-phase vs. out of phase chopping 30
Figure 15: Varying chopped beam power, while other held at 40mw 32
Figure 16: Varying unchopped beam power 32
Figure 17: LED response 35
Figure 18: Lockin autophase results vs. average input power 36
Figure 19: Compensator setup 38
Figure 20: Broadened pulses measured with BBO crystal 39
Figure 21: Broadened pulses measured with amber LED 40
Figure 22: Normalized and zoomed plots (a) LED-based measurements and (b) BBO-based measurements with broadened pulses 42
Figure 23: 10x Magnification of OSRAM LE-A-QW9N LED 44
Figure 24: Autocorrelation measurement from OSRAM LED 44
Figure 25: Carrier generation from SHG in (a) traditional autocorrelation setup with photodiode (b) LED detector 49
Figure 26: Sample interferometric autocorrelation trace [1] 50
Figure 27: Simulated Propigation of Pulses in Semiconductor Slab 52
Figure 28: Basic model output 54

Figure 29: Simulated response to varying average beam power (a) without FCA effects (b) with strong FCA effects 58
Figure 30: Simulated autocorrelation measurements with various FCA cross sections 59
Figure 31: Simulation result in agreement with cree data 64
Figure 32: Simulation results in agreement with OSRAM data 65
Figure 33: Simulated autocorrelations for various pulse widths 68
Figure 34: Intensity autocorrelation setup. 76
Figure 35: Direction of Propagation Through SHG Crystal 77

CHAPTER I

Introduction

1.1 Motivation

Optical autocorrelation techniques are well-known in labs where ultrashort pulsed lasers are operated. These techniques allow the pulse width of a laser to be accurately determined. However, the usefulness of these systems if offset by their difficulty of alignment and expense of materials. The second-harmonic generation (SHG) crystals required in traditional autocorrelation setups are particularly troublesome. The crystals alone can have costs approaching the thousand dollar mark, and commercial autocorrelation systems sell for prices on the order of $10,000. Researchers who choose to assemble custom autocorrelators will find the alignment and focusing of the optics difficult and time consuming, since correct alignment can often be confirmed only through the lengthy process of searching for a very weak signal, and then fine-tuning to improve performance. For these reasons, it is desirable to replace the SHG crystal with a cheaper, more robust, and easier-to-align device. Light-emitting diodes (LEDs) have been used for this replacement. They have been demonstrated to possess a nonlinear response to ultrafast laser pulses, and they provide feedback during alignment which makes setup much easier. However, we have observed erroneous reporting of the laser pulse widths using these LED-based autocorrelators, which throws the accuracy of this new method into question. These results stand in contrast to the consensus of previous works. However, no complete theoretical principle of

operation has yet been developed that could explain the observed errors. Such an explanation is necessary if these devices are to be used reliably in autocorrelation systems. Perhaps more importantly, the properties of LED-based autocorrelators and the resulting measurements lend themselves to a very useful technique for quickly finding the point of zero delay in an optical experiment. The usefulness of this technique is not dependent upon the accuracy of the pulse width measurement. Additionally, it can be constructed at a very low cost and aligned extremely easily. The benefits and methodology of this system are explored in later chapters.

1.2 Previous Work

Previous works have reported the use of light-emitting diodes (LEDs) and photodiode detectors to replace SHG crystals in autocorrelation systems, citing accurate measurement of pulses as short as 6 fs [1]. However, the theoretical knowledge of why these measurements are possible is lacking in the literature. Several groups have demonstrated accurate autocorrelation using LED detectors and photodiodes [1], [2], [3], [4]. However, none have posed detailed theories on the physical systems acting to produce these measurements. Any analysis that does exist is limited to either speculation about several possible sources of nonlinearity [5], or to a theories of nonlinear carrier generation in homogeneous semiconductor materials [6]. This is perhaps due to the fact that almost all previous experiments produced autocorrelation measurements in excellent agreement with the traditional SHG-based systems. These authors therefore knew that a second-order nonlinear mechanism similar to that of the SHG crystals was at work, and had little need to speculate on the exact mechanism involved. However, reports do exist which show disagreement between LED and SHG-based autocorrelators [7]. This suggests that additional mechanisms exist in *some* LEDs, and that these mechanisms depart from the pure second-order nonlinearity which previous authors assume in the LEDs.

1.3 Current Work

The works listed above prove that optical autocorrelation can be performed with LEDs and other similar devices, but they do little more. The existence of reports which show error between LED and SHG-based measurements also highlights a danger in using LEDs as autocorrelation detectors. Since the source of these errors is unknown, one can never be sure if the LED chosen for an autocorrelation system will be accurate or not. It is therefore important to discover the cause of these errors so that inaccurate LEDs can be avoided or the measurements from these LEDs can be corrected. This knowledge may also allow for the intelligent selection of diodes whose materials and/or construction allows the most effective measurements to be made by maximizing sensitivity, resolution, etc. The current work attempts to address this issue in two ways. First, a detailed set of measurements has been gathered to evaluate the performance of LED-based autocorrelators under a range of test conditions. This has been done with the hope that varying system parameters and observing the resulting changes in measurement can help to define the possible physical effects at work in these devices. Secondly, simulation models have been developed which attempt to match the collected experimental data. These models are based in the well-known carrier generation, lifetime, and transport theories of semiconductors, uniquely applied to reproduce the experimental data and validate the proposed mechanisms at work in the LEDs.

The most significant impact of this work is arguably the confirmation of the erroneously large full-width-half-max (FWHM) pulse widths as well as the observation of extremely wide "shoulders" in the autocorrelation traces when using LED-based autocorrelators. These are discussed in detailed in subsequent chapters. As stated previously, this result has been almost entirely unreported in the literature, and has serious implications for the use of this technology. These effects were found with varying severity in several LEDs, regardless of emission wavelength or manufacturer. This may be due to the increased complexity of modern LED

design. These factors are extremely detrimental to the use of LEDs in autocorrelation setups. The existence of the above effects without understanding of their causes means that any LED must always be tested against an SHG crystal's results before it can be trusted. However, these effects can be put to good use in other ways. The artificially wide autocorrelation peak coupled with the large width of the shoulders allows the total measurement to extend across ranges of up to 4 ps. This corresponds to a change in optical path length on the order of millimeters around zero delay. This is an extremely large distance in the context of typical optical setups which utilize variable delay (e.g. THz, pump-probe, etc). Additionally, the focusing of overlapping pulses onto the LED *does not require* the approximate position of zero delay to be known before acquiring a signal. This stands in contrast to other measurement techniques. For example, the alignment procedure for THz transmitter/receiver pairs, pump-probe measurements, and even SHG-based autocorrelators requires many test measurements to be made just to identify zero delay. When a weak signal is finally found, the measurement can be centered and the optics adjusted to peak the signal. Conversely, the direct electrical response of the LED to optical pulses provides real-time feedback during focusing. Each beam can be roughly overlapped by eye. Then photo-generated voltage or current from the LED can be used to maximize the focus and overlap without ever taking a measurement scan. This eliminates the need to perform numerous trial autocorrelations to observe the response of the system before adjusting the focus of the pulses. Sensitivity is high enough that this can be done using a simple voltmeter to measure the LED response. For these reasons, LEDs are extremely useful as tools to identify zero delay in optical setups, even if accurate FWHM measurements are not possible. The current work investigates this possibility of creating a robust "zero delay finder" device, as it will be referred to in subsequent chapters.

1.4 Outline

The information in the report is organized as follows:

Chapter 2 describes the basic concepts of LED-based optical autocorrelation. The purpose of this chapter is to familiarize the reader with the theory of optical autocorrelation. This knowledge provides a necessary context for understanding the research presented in the chapters that follow. The concepts outlined include the necessity of nonlinearity for autocorrelation measurements and the nonlinear mechanism at work in the LEDs. Chapter 2 also provides theoretically based discussion of the differences between LED-based and traditional autocorrelation techniques.

Chapter 3 provides a survey of previous research on this topic. The findings and theories of previous researchers are identified and analyzed.

Chapter 4 introduces the measurement techniques used in the current research and discusses the results. Comparisons are made to the results of other experiments listed in Chapter 3. Particular emphasis is placed on the signal shoulders and broadening of the FWHM reading compared to SHG crystal control measurements, which was not found in previous experiments.

Chapter 5 discusses the theories of carrier generation and collection which are thought to be responsible for allowing autocorrelation measurements with LEDs. Unfortunately, the manufacturers of the LEDs used in this research were unwilling to provide information on their exact structure. This makes definitive answers about the effects of device structure on the measurements impossible. However, common device structures are discussed and analyzed in light of the results presented in Chapter 4. This chapter focuses largely on explaining the unusual broadening and shoulders found in the measurements of this research. Information on specific LED structure proved difficult to obtain. However, the range of possible physical mechanisms is narrowed, a largely accurate model is developed, and promising avenues for further research are identified.

Chapter 6 summarizes the findings and discusses the usefulness of the observed measurements parameters for use in zero finding devices for systems involving optical delay.

CHAPTER II

Foundational Technique and Use of LEDs

2.1 Necessity of Nonlinear Response

Intensity autocorrelation of any signal is performed by overlapping the signal with a copy of itself and evaluating the result as a function of delay. In mathematical form, the autocorrelation function $A_c(\tau)$ is given by the following expression:

$$A_c(\tau) = \int_{-\infty}^{\infty} I(t)I(t-\tau)dt, \tag{1}$$

Where $I(t)$ is the optical signal that is to be evaluated, and τ is the delay between copies of the signal. For Gaussian pulses, this expression has the following solution:

$$A_{Gauss}(\tau) = I_0^2\sigma\sqrt{\pi}\exp\left(-\frac{\tau^2}{4\sigma^2}\right), \tag{2}$$

Where I_0 is the peak intensity of the pulse and σ is related to the FWHM value of the pulse by the equation

$$\text{FWHM} = 2\sqrt{2ln(2)}\sigma. \tag{3}$$

The derivation of this result, along with a more detailed overview of a standard autocorrelation system, can be found in Appendix A. There are several important implications of this result: The autocorrelation of a Gaussian pulse always possesses Gaussian form, and always has a FWHM

value exactly $\sqrt{2}$ times larger than the FWHM of the original pulse. This makes autocorrelation techniques extremely useful for pulses too short to be measured directly.

Equation 1 contains two operations that are not normally possible in optical systems: integration and multiplication of signals. The integration can simply be performed by reading the signal from a slow detector. If the detector's response is much slower than the duration of the two pulses, then its response will be proportional to the sum of all carrier generation over the entire two-pulse event. However, the multiplication of pulse intensities is much harder to achieve. This multiplication can only be achieved through nonlinear mixing of the signal and its copy. This is proved and the methods are further analyzed in Appendix A. It can be clearly seen that the need for this multiplication makes a nonlinear response central to the successful use of an autocorrelator. Any device intended to replace the SHG crystal in autocorrelators must possess a measurable nonlinear response.

Previous experiments have demonstrated the use of Light-Emitting Diodes (LEDs) to perform autocorrelation measurements, replacing both the SHG crystal and the photodiode detector of the traditional setup [5], [2]. Since SHG crystals can only perform conversion of light, an additional detector (usually a photodiode) is required to measure the second harmonic response from the crystal. However, the LEDs do not convert light to second harmonic. Instead, the rate of carrier generation is nonlinear with respect to optical intensity in the LED, and this produces a directly measurable voltage or current from the LED whose response is nonlinear with the incident intensity. Once these carriers are generated, the contacts built into the LED provide a means to measure them. This process will be explained in greater detail below.

2.2 Nonlinear Carrier Generation in LEDs

Nonlinear absorption occurs in many semiconductors for high-intensity light. One major mechanism for this nonlinear absorption is a process called two-photon absorption [8], sometimes

abbreviated as 2PA. In this process, a single transition occurs by absorption of two photons, as illustrated in Figure 1.

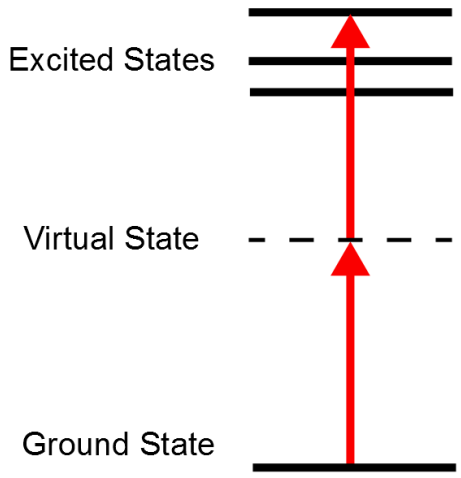

Figure 1: Two-photon transition

This transition involves a virtual state, which the atom cannot actually reside in. Therefore, both photons must arrive at an atom within an extremely small time frame (sub-femtosecond) for 2PA to occur. Therefore, the rate of carrier generation due to 2PA is related to the concentration of photons in a given area, or the intensity of light incident on the material. The total rate of carrier generation in a material is given by [8]:

$$\frac{dN}{dt} = \frac{\alpha I}{\hbar w} + \frac{\beta I^2}{2\hbar w}, \tag{4}$$

Where N is the carrier density (in cm^{-3}), α is the linear, single photon absorption coefficient (typically measured in cm^{-1}) and β is the 2PA coefficient (typically measure in $^{cm}/_{GW}$). Note that α is usually very small at wavelengths for which β is significant, since a large values of β are rarely found in materials with bandgap energy close to that of a single photon.

2.3 Use of Two-Photon Absorption for Autocorrelation Measurements

To illustrate the use of 2PA for autocorrelation measurements, a simple example can be analyzed. In this example, only a very thin layer of semiconductor material is considered, such that the intensity of light $I(t,z)$ is constant in z such that $\frac{dI(t,z)}{dz} = 0$. In this special case, the intensity reduces to $I(t,z) = I(t)$. The original optical pulse is divided into two pulses as normal, and both pulses are focused onto this thin layer of material. Under these assumptions, the rate of change in carrier density will be given only by Equation 4. Assume also that all produced carriers have an effectively infinite lifetime and they are readily transported to some current/charge detection device. In this case the entire two-pulse event is still much faster than the ability of the detector to resolve. Therefore the detector will simply collect the total number of carriers produced over the entire event. The final voltage/current read by the detector will then be proportional to the total carrier density, which can be found by integrating Equation 4:

$$S_{det} \propto N = \int_{-\infty}^{\infty} \frac{dN}{dt} dt = \int_{-\infty}^{\infty} \left(\frac{\alpha I(t)}{\hbar w} + \frac{\beta I^2(t)}{2\hbar w} \right) dt. \tag{5}$$

Assuming a Gaussian pulse as before, the total intensity incident upon the material layer is the sum of both pulses:

$$I(t) = I_0 \exp\left(-\frac{t^2}{2\sigma^2} \right) + I_0 \exp\left(-\frac{(t-\tau)^2}{2\sigma^2} \right). \tag{6}$$

Substituting into Equation 5 and solving gives the following result:

$$N = \frac{\beta \sigma \sqrt{\pi} I_0^2}{2\hbar w} \left(1 + \exp\left(-\frac{\tau^2}{4\sigma^2} \right) \right) + \frac{2\alpha I_0}{\hbar w} \sqrt{2\pi}\sigma. \tag{7}$$

There are three terms present in Equation 7. Two of the terms are constants in τ, and do not alter the FWHM value of the signal. The form of the exponential term is both Gaussian and identical to the form of Equation 2, proving that an autocorrelation trace $\sqrt{2}$ times wider than the original

pulse will also be measured when using an LED detector. The additional terms in this result are discussed below.

2.4 Comparison to Standard SHG Crystal Autocorrelators

Equation 7 contains the same Gaussian profile seen in traditional autocorrelation measurements. However, it also contains two extra terms. It is important to note that these terms are independent of τ. They are constants in the autocorrelation function. This causes one of the primary differences between LED and SHG crystal autocorrelation traces: The signal is offset from zero, as shown below:

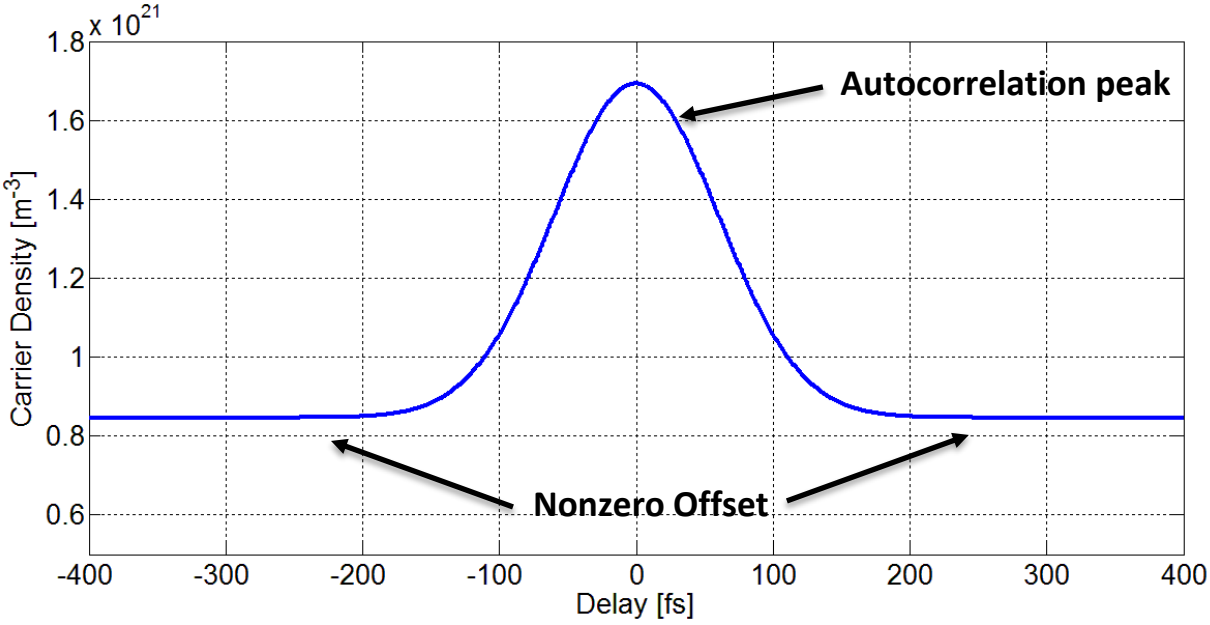

Figure 2: Results of analytical autocorrelation solution

This offset is due to the fact that the pulses are focused directly onto the collection device (the LED). Therefore, LED-based systems do not have the ability to reject pulses with no overlap from detection that is found in SHG-based systems. Even when the pulses are completely separated, both single and two-photon processes will still generate carriers, and these carriers will

be detected by the measurement device. This produces a constant signal because the number of carriers generated does not change unless pulse overlap occurs. *Figure 3* illustrates this.

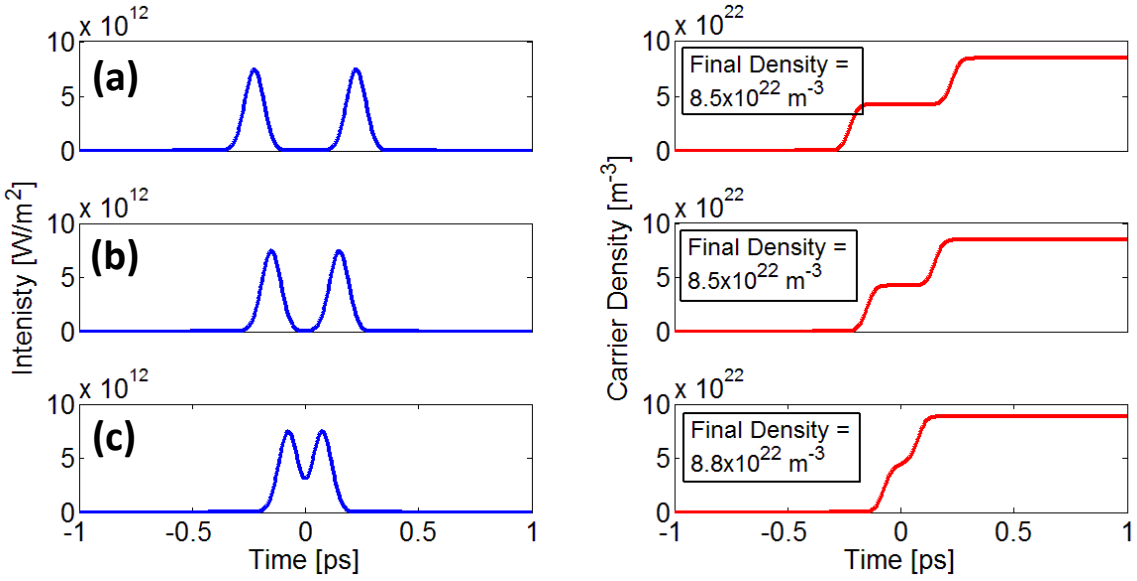

Figure 3: Intensity profiles and resulting carrier generation for (a) large separation, (b) reduced separation, (c) partial overlap. Notice that the final resulting carrier density does not change until overlap occurs.

When the pulses do overlap, the nonlinearity of the two-photon process increases the total number of generated carriers. This allows the autocorrelation function to appear on top of the offset.

CHAPTER III

Survey of Previous Research

A number of successful experiments have been performed to verify the possibility of measuring ultrafast pulses with LED and photodiode-based autocorrelators. These experiments, which are discussed below, cover a range of pulse-width measurements, LED device structure, and LED materials. Pulses as short as 6 fs have been measured with GaAsP photodiodes [1]. This experiment showed nearly perfect agreement with measurements taken of the same pulse using the traditional SHG approach with a BBO (beta barium borate) crystal.

Pulses of 800nm light as short as 80 fs have also been measured using AlGaAs LEDs [5]. The authors of this report performed several tests on the LED, demonstrating no response at very low optical power and saturation at high optical power. A successful autocorrelator was built and tested using the LED, and speculation was made as to the mechanism allowing the necessary nonlinearity: both two-photon absorption by itself and second harmonic generation followed by single photon absorption of the resulting light were proposed as possibilities. This report demonstrates the use of LEDs in autocorrelation systems, but also provides speculation about the sources of nonlinear response in the LED that is absent from most other reports. However, the report does not perform any analysis beyond this simple speculation.

More recently, successful interferometric and intensity autocorrelations have been performed with amber, GaAs-based LEDs [2]. The nonlinear response of red GaAs-based LEDs as well as blue and green GaN-based LEDs was also measured by [2]. These devices were also found to have nonlinear responses to 800 nm light, but this response was weaker than that of the amber LED. This implies that these LEDs could have also produced measurable autocorrelation signals. However, autocorrelations were not performed with these LEDs.

The above results clearly demonstrate that autocorrelation measurements can be obtained using LEDs and photodiodes as detectors. Furthermore, these experiments imply that a wide range of structures can be used successfully, although unknown parameters cause some devices to work better than others. While no specific theories have been developed, several other results give clues as to the important factors at work. These are listed below.

3.1 Other Device Structures

Several other 2PA-based devices have been used to measure autocorrelations. For example, waveguide structures have been used [9], [10]. This type of device allows the light to travel through a longer structure, increasing the exposure of the material and thus generating more carriers from 2PA. Contacts plated onto the waveguide can be used to collect the generated carriers similarly to the use of the LED contacts. It is also worth noting that some single-photon absorption was still observed in this setup [9]. Unfortunately, the waveguide approach has several disadvantages. Most importantly, it requires custom fabrication, and therefore does not provide the cost savings which make LED-based autocorrelators attractive. Additionally, the alignment of such devices can be difficult and sensitive to the quality of coupling [9]. While they do not relate directly to LED-based measurements, these reports provide useful information on the linear and nonlinear absorption parameters in semiconductor materials similar to those used in LED construction.

Quantum well structures have also been used to perform 2PA-based autocorrelations [11]. These structures have been demonstrated to greatly increase the 2PA coefficient β, with estimated values in the range of $5 \times 10^3 \mathrm{cm/GW}$. As noted in [11], this is approximately two orders of magnitude higher than the 2PA coefficient for pure GaAs [12]. It is also noted in [11] that the ideal structure for maximum sensitivity in a device may place a lower limit on the resolution of the autocorrelation. This limit is caused by intersubband scattering of carriers [13]. This report is particularly interesting, since modern LEDs contain many active layers, and often utilize multiple quantum well layers. The fact that this structure has the ability to significantly increase the 2PA coefficient is promising, as quantum wells are often used in light emitting devices such as LEDs.

These results reveal several important factors. First, the *ability* of a device to produce an autocorrelation signal is fairly independent from the device's structure. Measurements are possible as long as the device is made from a semiconductor with sufficiently large β and possesses contacts to collect the generated carriers. However, these results also reveal that, while autocorrelation is possible across a wide range of device structures, the *quality* of these autocorrelation measurements can be massively improved by various factors in the devices construction. Elements such as quantum wells can greatly enhance the 2PA coefficient β that is critical to these measurements, while structural modifications can improve the efficiency of carrier generation and collection.

3.2 Broadening and Other Factors

The LED-based autocorrelators constructed as part of this research produced erroneously broadened FWHM measurements and signal shoulders, but this result is largely absent from the literature. Most previous works have shown the ability for LEDs and photodiodes to faithfully measure very short pulses. Importantly, one experiment involving *photodiode* detectors did not

[7]. The FWHM measured in this experiment (using a GaAs Schottky barrier photodiode) was between 1.75 and 2.19 times larger than the value measured using an SHG crystal. This work again illustrates that the structure and composition of the measurement device can play a big role in the capability of the autocorrelator built thereupon. Additionally, there is a minimum time resolution that is possible using 2PA-based techniques. This time resolution is related to the duration time of the two-photon transition [14]. This result makes sense intuitively, since the device cannot respond to events which happen faster than the carrier generation mechanism.

3.3 Summary

It is clear from the works cited above that the ability of LEDs and photodiodes to create autocorrelation measurements has been thoroughly proven. Measurements of several different styles have been performed across a large range of wavelengths with a large number of different devices. The basic mechanisms governing carrier generation have also received some theoretical treatment. However, the literature is almost entirely absent of any attempt to explain inaccuracies, broadening, or shoulders, even by the minority of authors who observed these effects.

CHAPTER IV

Experimental Results

An important goal of this work was to provide a more detailed characterization of LED-based autocorrelators than previous studies have given. A number of experiments were performed to test the performance and response of these systems under many different conditions. It should be noted that the methodology involved in setting up and focusing the LED-based autocorrelators evolved throughout this research. This caused certain differences between the various data sets, which will be discussed below. However, the most important information can be gathered from the trends within each dataset. These experiments are described and discussed below.

4.1 Preparation of LEDs

Several LEDs were purchased for testing as autocorrelation detectors. However, modifications were required before these LEDs could be used. LEDs are typically packaged inside thick epoxy lenses which are intended to help spread light from the LED. These lenses are problematic for autocorrelation for several reasons. Most importantly, this thick layer of epoxy would interfere with the transmission of pulses into the LED die. The epoxy would be the thickest material in the system, and *could* cause significant dispersion of the pulses, resulting in inaccurate measurements. However, Kramers-Kronig relations would require significant absorption at 800 nm for this to occur, and this is unlikely in LEDs designed to operate in the amber and red spectrum. Unfortunately this is not the only problem caused by the epoxy. The lens dome formed

by the epoxy distorts the image of the LED die. This makes focusing of the pulses onto the die very difficult. For these reasons, much of the epoxy dome was removed.

Ideally, all of the epoxy would be removed, leaving the LED die and its gold wire bond exposed to air. Fuming nitric acid is sometimes used to remove molding from integrated circuits (IC's), leaving the wire bonds and internal dies intact for inspection. However, this approach is expensive, dangerous, and could destroy the LED dies if improperly applied. Instead, the epoxy domes were ground down as far as possible without destroying the wire bond or the LED die, as shown in Figure 4. This left a very thin layer of epoxy over the die. After the rough grinding, the now flat surface was polished using a rouge polishing compound to maximize transmission of light. This approach minimized any possible dispersion and transmission problems and made the focusing of pulses onto the die significantly easier.

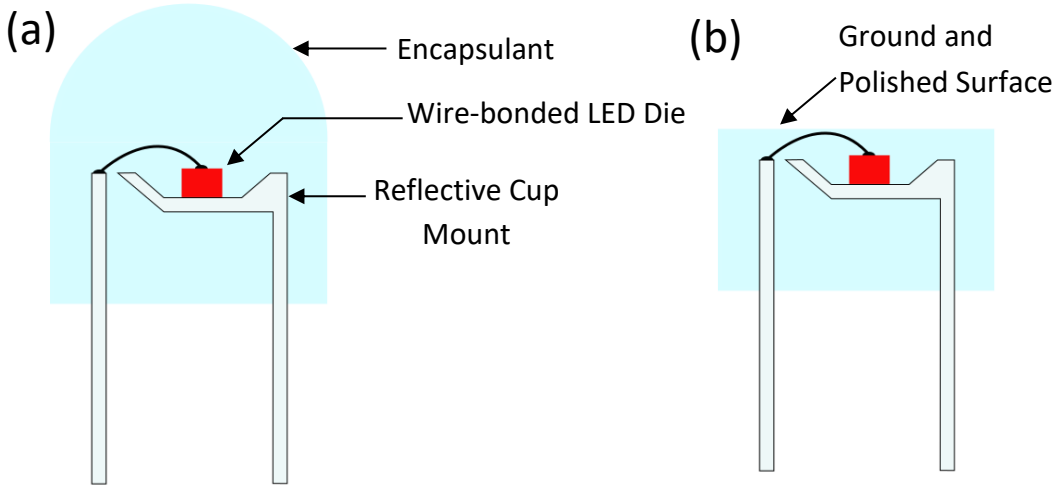

Figure 4: Through-hole style LED. (a) Unmodified construction (b) After grind and polish.

4.2 Basic Autocorrelation Measurements

Before testing LEDs, the performance of the autocorrelator was benchmarked by using a known and reliable detection scheme: a BBO crystal, a blue filter, and a photodiode. This was done because the exact pulse width of the laser was unknown, and a trusted reference measurement

was needed to validate the LED autocorrelation measurements. There are many autocorrelation setups to choose from, but an intensity autocorrelation setup was chosen for these tests. The primary benefit of such a system is the minimization of glass through which the pulses must pass. An interferometric autocorrelator requires an additional beam splitter, which can introduce further dispersion to the pulses. Additionally, the basic intensity autocorrelation setup allows for individual adjustment and focusing of each beam path. This simplifies the process of aligning the device for a measurement, making results easier to obtain.

The setup is shown in Figure 5. Variable pulse delay was achieved using a hollow corner-cube reflector mounting on a motion stage, and final focusing of the beam was achieved using a parabolic mirror. Note that mirrors M2 and M3 serve to lengthen the beam path so that both positive and negative delays are possible.

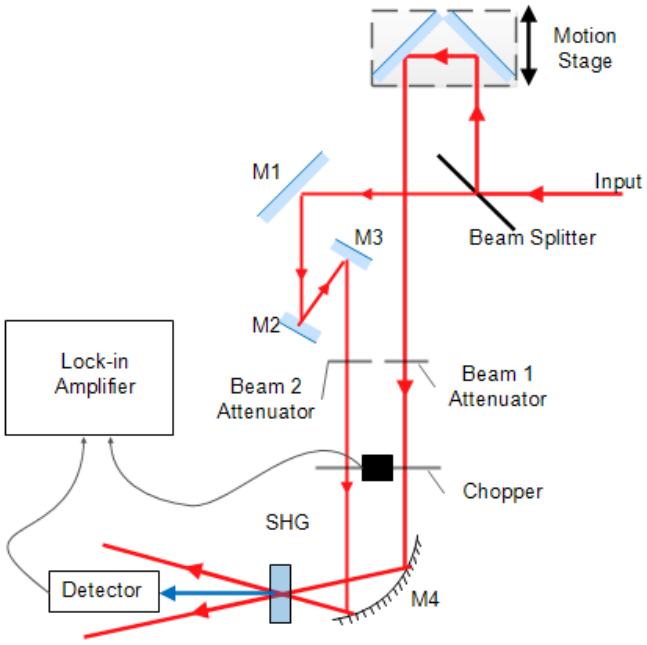

Figure 5: Intensity autocorrelator with BBO crystal

The attenuators shown in Figure 5 allowed the average power of each beam to be precisely controlled. This was important for many of the tests performed, which are discussed below. The chopper is shown to be placed in the path of both beams. However, as will be discussed later, its

position was varied for different measurements, sometimes chopping only one beam. This change is noted for the relevant experiments below.

The chopper fed a reference signal to the lock-in amplifier. This allowed the amplifier to filter out any signal which was not modulated at the chopper frequency, greatly reducing noise in the measurements. The amplifier and linear motion stage were controlled by a data acquisition program written in LabView, a data acquisition software suite developed by National Instruments. This program moves the stage by a specified distance (in 1 μm steps for most measurements) to change the delay between pulses. The stage pauses after each motion to allow time for vibrations to settle, then records the signal reported by the amplifier at that position.

After successfully generating autocorrelation signals using the BBO crystal, the LED detectors were tested. To do this, the setup of Figure 5 was modified as shown in Figure 6. The BBO crystal and photodetector were removed and replaced by an LED. The contacts of the LED were connected to the lock-in amplifier via coax cable, allowing for a direct measurement of the voltage generated by the LED. This easy interchange of detectors is another valuable advantage of this system, allowing any LED detector measurement to be quickly verified with a traditional SHG-based autocorrelation.

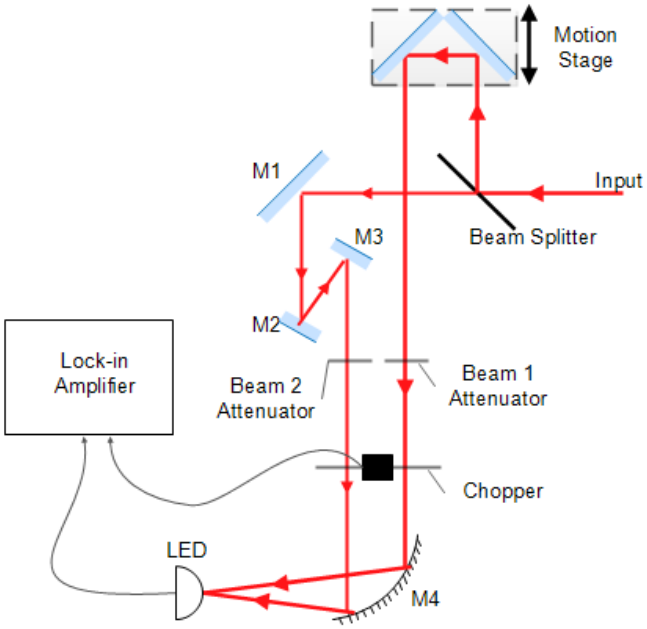

Figure 6: Intensity autocorrelator with LED

The initial set of data taken from these two systems consisted of autocorrelation measurements taken using the BBO crystal as well as four separate LEDs. The LEDs where all AlGaAs-based dies manufactured by Cree, and had emission colors of amber, red, blue, and green. The raw results of these measurements are shown in Figure 7. The green LED is not plotted, since no measurable signal was found when using it as a detector.

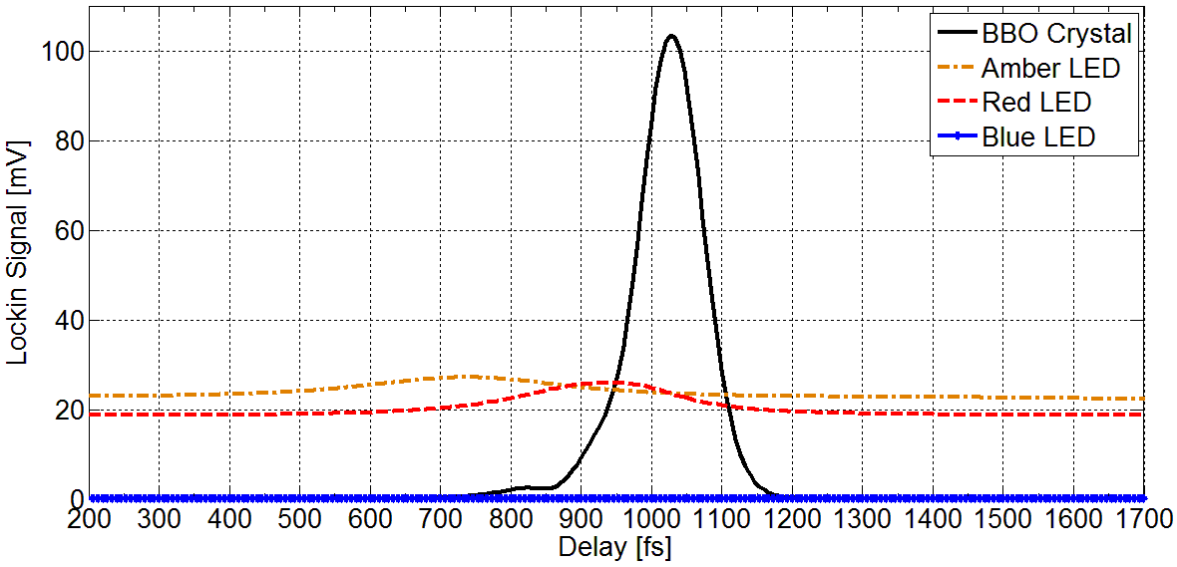

Figure 7: Initial raw autocorrelation measurements

Figure 7 provides a useful visualization of the differences between SHG-based and LED-based autocorrelation measurements. It is clear that the SHG-based method is significantly more sensitive than any of the LED-based methods, with an amplitude approximately one order of magnitude higher than even the best LED-based measurement. This is likely due to the fact that the photodiode detector used for the SHG-based system is better optimized for carrier generation than the LEDs. However significant alignment efforts were also invested to maximize the signal from the SHG-based measurement, and this likely influenced the system sensitivity. Despite this difference in amplitude, the LED-based measurements are still easily readable. Figure 8 shows the LED-based measurements scaled and offset to match the base and amplitude of the SHG-based measurement. The amber, red, and blue LEDs were multiplied by a scaling factor of approximately 20, 14, and 1250, respectively. This makes comparison of the autocorrelation traces much easier.

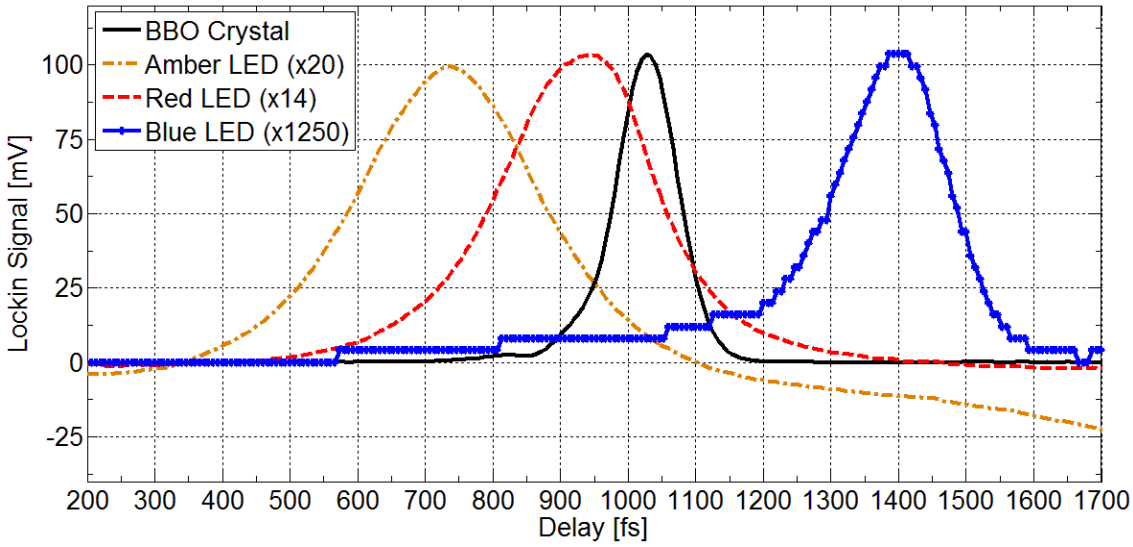

Figure 8: Scaled autocorrelation traces

Several noteworthy features appear in Figure 7 and Figure 8. First, it is apparent that the blue LED produces the weakest signal. The amplitude is so small that the autocorrelation signal appears non-existent when compared to the other measurements in the raw data of Figure 7. Since the lock-in amplifier range settings were not changed between measurements, this small amplitude caused poor resolution in the voltage of this measurement. However, the time resolution is still sufficient for analysis of the important measurement features.

Another important feature of these measurements is the presence of "shoulders" in the measurements. These shoulders do not appear in Figure 7 or Figure 8 because the range of delays used was too low. Longer scans revealed that the autocorrelation peaks were in fact sitting on top of a larger signal. An example of these longer scans is shown for the amber LED in Figure 9.

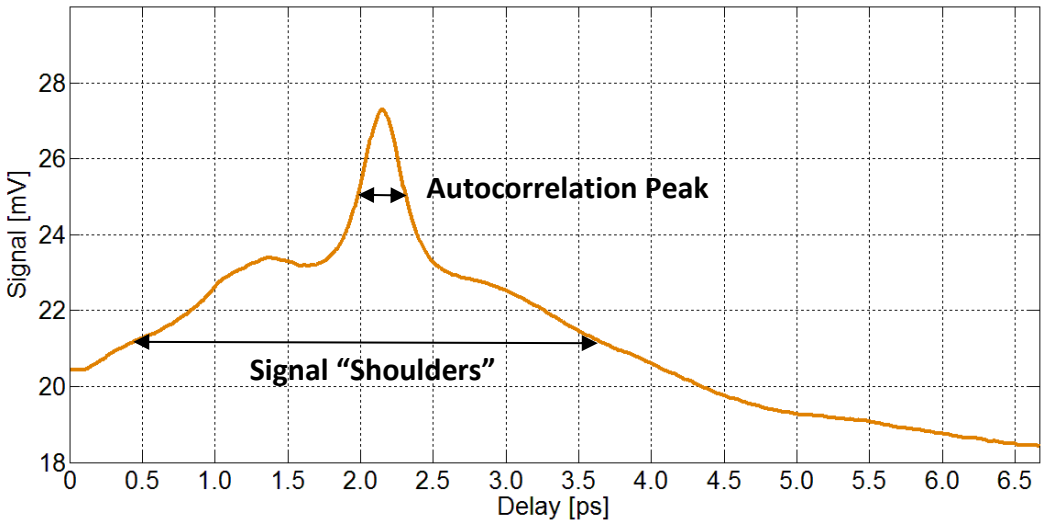

Figure 9: Wider scan of original measurements with amber LED

In addition to the shoulders, significant broadening was seen in all of the LED-based measurement devices. The measurement acquired with the BBO crystal has a FWHM value of approximately 106 fs, implying and actual pulse width of 75 fs. Figure 8 clearly shows that the measurements made using the LEDs are significantly wider than the measurement made using the BBO crystal. The FWHM values obtained from the amber, red, and blue LEDs are 293 fs, 260 fs, and 190 fs, respectively. These value indicate actual pulse widths of 207 fs, 183 fs, and 134 fs. The amber LED shows the largest broadening compared to the BBO crystal measurement with a factor of 2.76 increase.

The shoulders and broadening shown in the above figures are extremely important. To our knowledge, these effects have been seen only once before with any type of semiconductor based detector [7], and never in measurements taken with LEDs. They are obviously important, and seemingly common, features observed in autocorrelators based on modern LEDs. This behavior is critical to the utility of LED-based autocorrelators, since inability to accurately measure the FWHM value of a pulse renders such a device useless. On the other hand, the large delays over which a signal exists in these measurements increases the usefulness of these devices for finding zero delay, which does not require accurate determination of the FWHM value. This

concept will be discussed in subsequent chapters. In either case, more information is required. In order to further investigate this broadening, a number of additional experiments were undertaken.

4.3 Amplitude Testing

The next logical step was to confirm that the measured traces above were in fact autocorrelation measurements, and then to test the limits of these measurements under various input conditions. In order to confirm that the observed measurements are in fact autocorrelations resulting from the overlap of both beams, each beam was blocked and measurements were taken with only one beam active. This resulted in a loss of the autocorrelation signal as expected, indicating that the observed peaks in the measurements do result from the interaction of both beams, and are therefore actual autocorrelation signals. These tests were performed with a wider scan range, revealing the signal shoulders mentioned above. The signal shoulders do not follow the same Gaussian profile as the autocorrelation peaks. Therefore, they are most likely due to an additional mechanism. An attempt was made to remove these shoulders by lowering the average beam powers. It was theorized that the effects of the additional mechanism might vanish with weaker beams. The results of these tests are shown for several average powers in Figure 10. Note that each beam was held at the listed power.

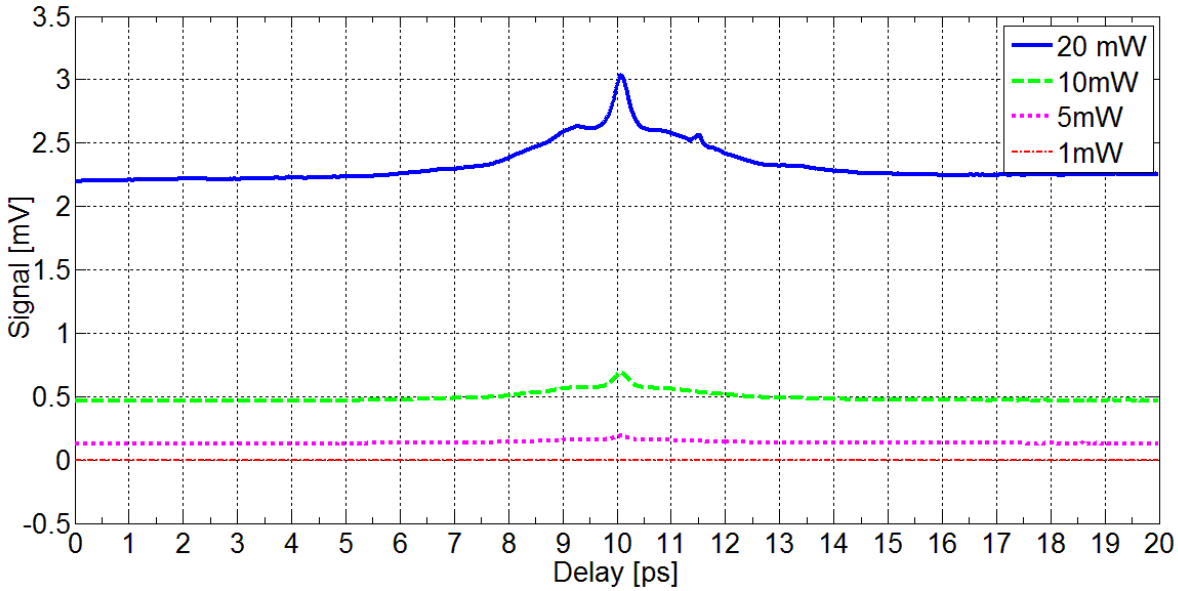

Figure 10: Autocorrelation signal dependence on average beam power

Note that no measureable signal was found at 1 mW per beam. The increase in signal amplitude is nonlinear as expected. By comparing the amplitude of the signal floors, it can be seen that the increase approximately follows the relationship $A = .0055P^2$, where A is the floor amplitude and P is the average input power per beam. Unfortunately, the difference in amplitude between measurements makes comparison on a single figure difficult. Figure 11 shows the highest power (20 mW per beam) and lowest power (5 mW per beam) measurements alone. Note that the 5 mW measurement has been multiplied by a constant factor of approximately 17 for comparison. It can be seen that the shoulders remained largely unnaffected by the factor of 4 reduction in power from 20 mW to 5 mW. The autocorrelation peak accounts for a slightly larger portion of the overall signal amplitude for the 5 mW measurement, but the two measurements are otherwise posses identical shapes.

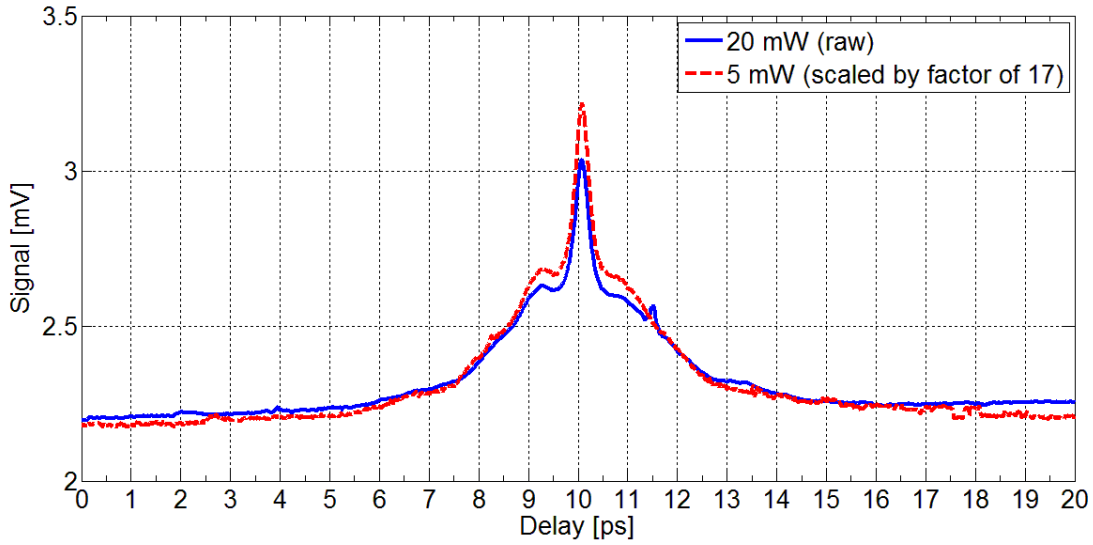

Figure 11: Autocorrelation with 20 mW average power per beam

All tests showed the same FWHM of 315 fs (not including the shoulders). The exact shape of the shoulders, including the dip just before the autocorrelation peak, are visually identical in all measurements and the ratio of shoulder height to autocorrelation signal height changes very little between measurements. This indicates that the shoulders do not result from a mechanism that can be minimized by lowering average beam power, since both the shoulders and the autocorrelation peak remained present until power was too low to produce any signal. This demonstrates that the mechanism causing the shoulders is not dependent upon the average beam power, and that it is present for all intensities high enough to allow a nonlinear response. This does not necessarily mean that the shoulders are due to the nonlinear response. It does however indicate that the strength of the mechanism causing the shoulders is similar to that of the nonlinear response or that the mechanism requires the nonlinear response to be present in order to generate shoulders.

4.4 Variable Beam Testing

The robustness of the autocorrelation measurements was further tested by varying the average power of each beam individually, with the other held constant. To do this, the attenuators shown in the setup of Figure 6 were adjusted to vary the average beam power. This power was measured using a power meter placed in the beam path. For each beam, measurements were taken

at several power levels while holding the opposite beam power at approximately 40 mW. The results of these measurements are shown in Figure 12 and Figure 13. These figures show an unexpected difference in behavior. Both beams contribute carriers, and it is the nonlinear increase in the number of carriers generated that creates the autocorrelation signal when overlap occurs. Therefore, reducing the power of either beam should lower the signal floor and reduce the amplitude of the autocorrelation peak. This behavior was observed only when varying the power of beam 2 as shown in Figure 13, but not when varying the power of beam 1 as shown in Figure 12.

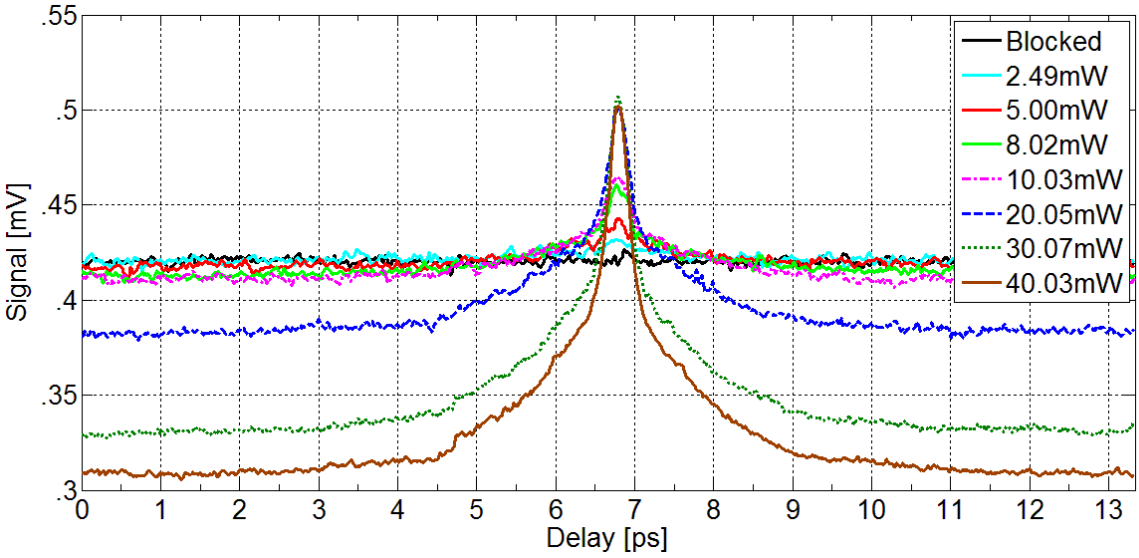

Figure 12: Varying beam 1 power with beam 2 power held at 40 mW, both beams chopped.

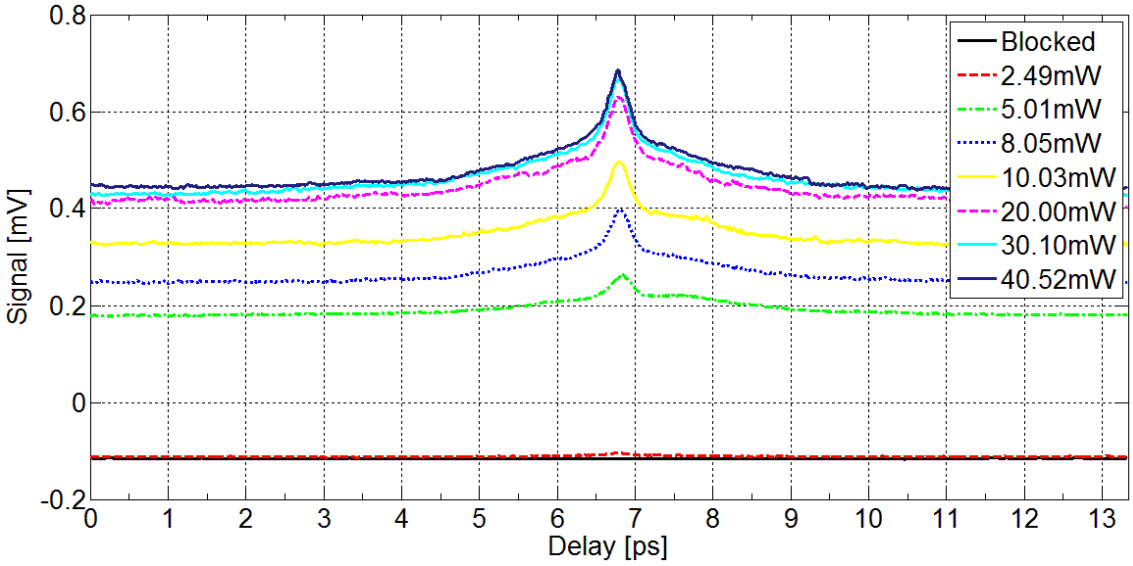

Figure 13:Varying beam 2 power with beam 1 power held at 40 mW, both beams chopped.

The amplitude of the autocorrelation peak does reduce as expected when the power of beam 1 is reduced. However, the signal floor rises. The floor of the signals in Figure 13 also reduce to negative values when beam 2 is at very low power or blocked entirely. This does not make sense, since beam 1 should still be generating carriers and producing a positive floor. Another problem is that the two sets of data should converge to become identical when the power of both beams is 40 mW. Instead, the signal floor in Figure 13 falls to a lower value than the floor in Figure 14, even though the power of both beams was identical for these two measurements. Note that the amplitudes of the measurements do become roughly equal in spite of this. These anomalies led to the discovery of a subtlety in the experimental method involving the placement of the chopper. Originally, both beams were chopped simultaneously. However, poor alignment of the chopper

can easily cause each beam to be chopped with a different phase. This is illustrated in Figure 14.

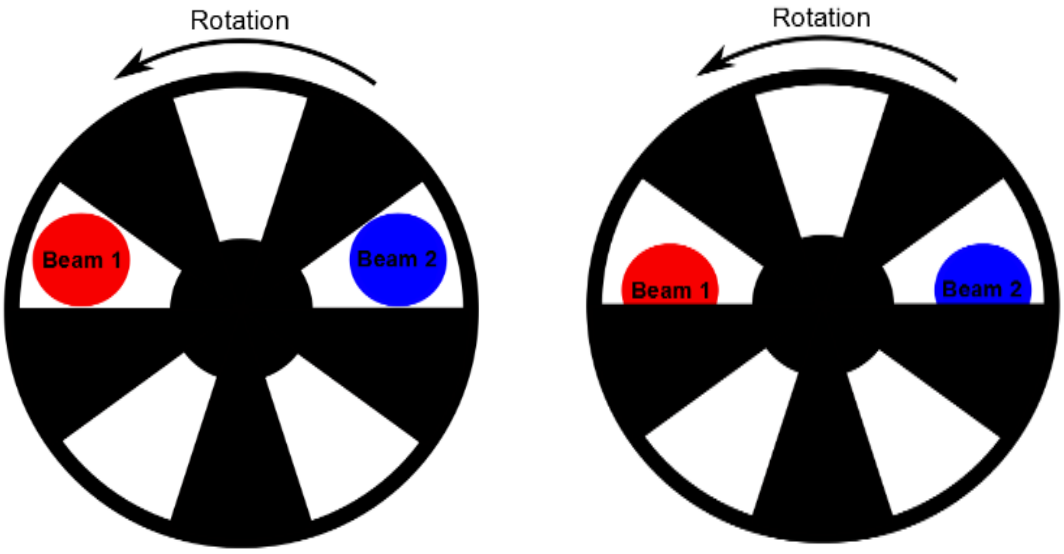

(a) Beams exposed and covered at the same time. Chopping is perfectly in phase.

(b) Beam 1 is exposed as beam 2 is covered. Beam 2 will be mostly covered when Beam 1 is fully exposed, and chopping will be out of phase.

Figure 14: (a) In-phase chopping (b) out of phase chopping

When the chopper is perfectly aligned as shown in Figure 14(a), both beams are blocked/unblocked at exactly the same time. Conversely, the chopper can be aligned so that one beam becomes blocked as the other beam is unblocked. This is shown in Figure 14(b). In this case the beams can be chopped up to 180˚out of phase, depending on how severe the misalignment is. In this case, according to the usual technique, the amplifier phase is adjusted such that it is referenced to 0°˚ when one *or the other* beam is perfectly centered through a window of the chopper. By the signal processing method of the lock-in, if the second beam is out of phase (in the range of 90°° to 270°˚ with respect to the center of the window), contributions to the signal from that beam are assigned negative value. Note that an autocorrelation signal would not be possible if the beams were chopped exactly 180° out of phase, since overlap of the pulses from each beam would then be impossible. However, partial out-of-phase beam chopping can

explain the anomalous features of the figures. In this case, it is apparent that the amplifier signal was adjusted to beam 2 and beam 1 was assigned a negative contribution. Therefore, when beam 2 is dominant, the highest signal floors are seen. As beam 1 grows stronger, the floor of the signal is reduced by its negative contribution. However, the amplitude of the autocorrelation peak grows. This is because there is overlap between the pulses which make up the beams as the delay approaches zero. Those pulses from beam 1 which are not blocked by the chopper gain the modulation of beam 2 due to their overlap, and are counted with positive value by the amplifier. This is why the amplitudes of the autocorrelation peaks are still able to increase as beam 1 grows stronger, even though the floor decreases. This also explains why many of the measurements in Figure 12 have approximately the same value for the autocorrelation peak. The negative values seen in Figure 13 are also explained by out-of-phase chopping. When beam 2 is fully blocked or extremely weak, the negative contribution assigned to beam 1 causes the measurement to appear as a negative value. As the power of beam 2 increases, it begins to dominate and the measurement becomes positive. The floor continues to rise as beam 2 grows stronger.

To confirm the theory presented above, the chopper was moved so that it chopped only one beam. Under this new configuration, carriers from the un-chopped beam alone should be disregarded by the amplifier as noise. When the pulses overlap, the second beam effectively mixes with the first, which is modulated, and thus the increase in signal is recorded. This modified setup should cause consistent behavior when varying each beam. Figure 15 and Figure 16 show the same measurements taken with the chopper on only one beam. In each measurement, the power of one beam was varied while the other beam was held constant at 40 mW.

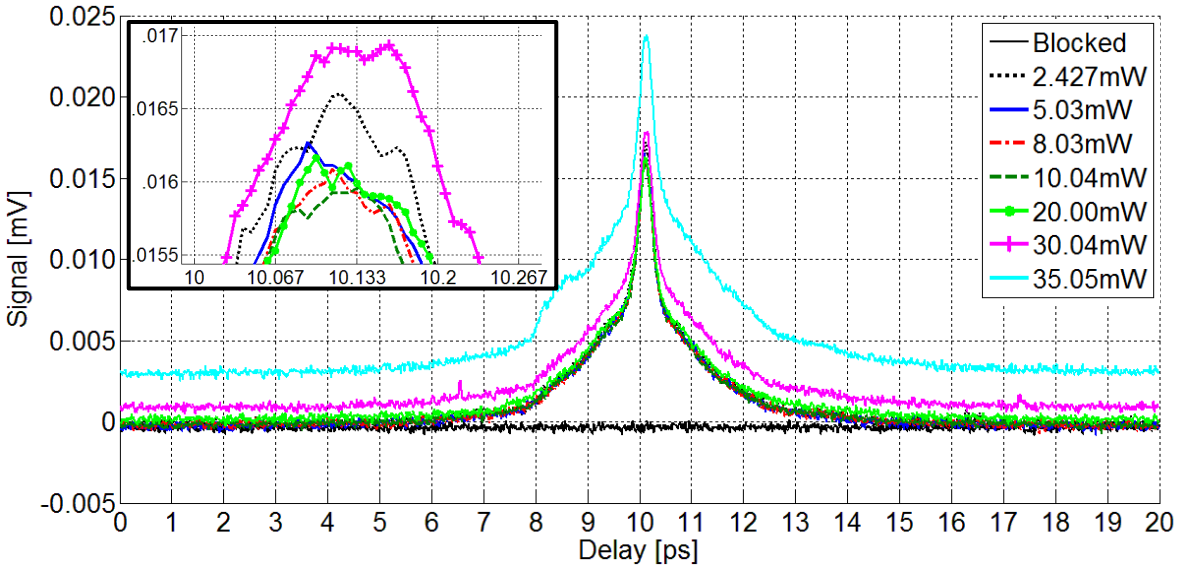

Figure 15: Varying chopped beam power, while other held at 40 mW. Plot markers added to inset for clarity.

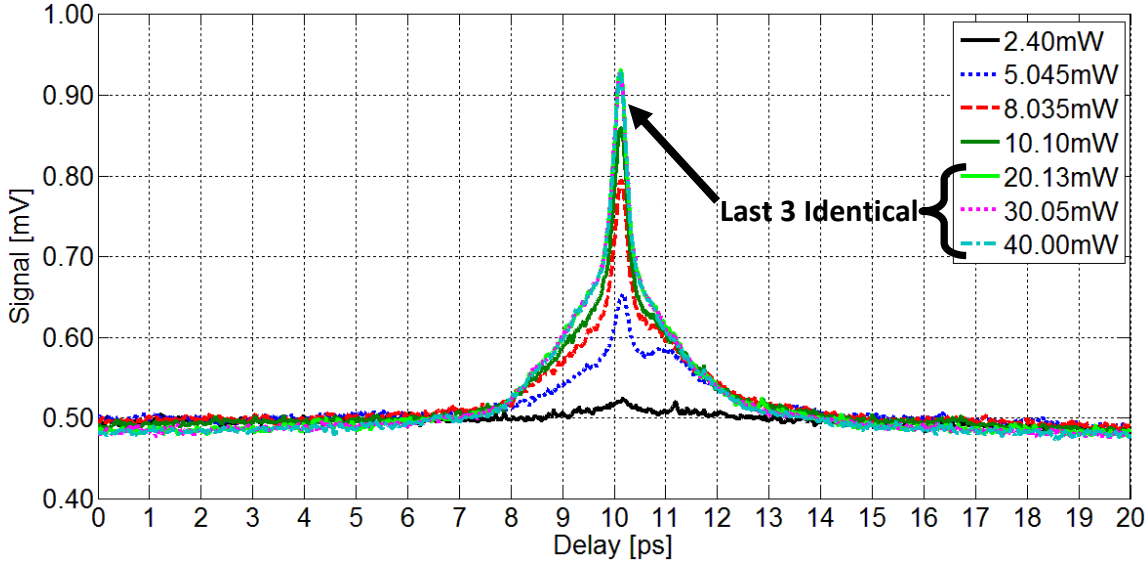

Figure 16: Varying unchopped beam power

Figures 14 and 15 show some of the expected behavior, but still have problems. No voltage is recorded by the amplifier when the chopped beam is blocked. This is expected even though the unchopped beam is generating carriers in the LED, since the unchopped beam has no modulation. However the amplitude of the autocorrelation peaks do not change significantly as the chopped

beam power increases. In fact, the signal initially falls, very slightly, as the chopped beam power increases (illustrated in the inset of Figure 15). The signal saturates at a minimum value around 10 mW, and then then begins to rise as the power of beam 1 continues to increase. This trend is also present in the signal floor, but it is less obvious and harder to observe.

The results from varying the unchopped beam behave as expected. When the unchopped beam is completely blocked, no autocorrelation appears as expected, but a nonzero voltage is still detected due to the modulated carrier generation of the chopped beam. The signal floor does not rise from this value as the power of the unchopped beam increases, but the amplitude of the autocorrelation peak does increase. This is expected, since the unchopped beam has no effect on the signal except through mixing with the modulated beam, and this occurs only when the pulses overlap to produce the autocorrelation peak. The signal amplitude appears to saturate after the 20 mW measurement. This is not unexpected, and is verified by our other experiments (see section 4.5). The only problem with the measurements shown in Figure 16 is the fact that they do not converge with the measurements from Figure 15. The final measurement in each of these sets was performed with both beams at 40 mW. Therefore, these two final measurements should be identical, but they the peak in Figure 15 is approximately 35 times lower than the peak in Figure 16. This problem is likely due to a change in the focus of light on the LED when additional attenuators where added to the unchopped beam to allow further control of its power.

The unexpected behavior seen in the amplitude and floor dependence of Figure 15 is worthy of further discussion since it revealed still more subtleties of the technique. Saturation is a possible explanation for the nearly constant amplitudes observed, but it is unlikely, since the amplitudes of these measurements are orders of magnitude smaller than the amplitudes obtained while varying the unchopped beam. Instead, this was likely caused by phase-shifting of the electrical signal as power increased. Significant lock-in phase shift has been observed to occur as the average beam power increases, but this phase shift appears to saturate above 30 mW (see

section 4.5). A significant phase shift would negate any increase in recorded amplitude as the chopped beam power increased, and could have actually caused a small reduction as observed in Figure 15. As the phase shift began to saturate, the increase in signal amplitude would be able to overcome the effects of the phase shift, allowing the signals to rise from the minimum value. A possible explanation for the phase shifting is changes in the junction capacitance of the diodes as pulse power increased. This could change the electronic response time of the diodes, causing a delay in the electrical signal with respect to the chopper's reference signal. This would reduce the amplitude of the signals. This is discussed in greater detail in Section 4.5.

Suffice to say, the results revealed that comparisons between data sets must be cautiously approached and must account for every subtlety of the experimental technique. Nevertheless, several conclusions can be drawn from the experiments. First, every set of data showed the same form of autocorrelation signal. This signal consists of a primary autocorrelation peak situated on top of shoulders, which appear to not follow the same Gaussian curvature as the actual autocorrelation peak. The FWHM of the primary autocorrelation was identical to within experimental error for each measurement, and the shoulders were present regardless of adjustment to the power of either beam. This reveals that there is an additional mechanism present in the LED detectors that modifies the autocorrelation signals from their expected shapes. The fact that these shoulders do not follow a Gaussian profile suggests this is not related to the 2PA process, or any other nonlinear optical effect. Rather, some other effect is allowing the pulses to interact either optically or electrically at larger delays than theoretically expected. This effect is discussed and replicated in Chapter 5. The data also reveals that the autocorrelation signal is extremely robust when LEDs are used as detectors. Large signals are still obtained even with either beam significantly weaker than the other. While amplitudes and floors may shift, the FWHM reading is unchanged. Finally, saturation was observed in the measurements. This fact combined with the large signals detected at lower powers suggests that high power beams are

unnecessary and even undesirable when using LED detectors. However, this saturation does not affect the FWHM value of the measurements, so there is no need for concern if higher power beams are used.

4.5 Saturation Tests

The response of the LEDs to average input power was tested next. This was done in the hope that possible causes of the broadening and shoulders could be revealed. In addition to this, the general response of the LED as a function of average beam power was desired in order to create a basic model which matched the data. If an equation could be fitted to this response, the data could possibly be replicated. To perform this experiment, one of the autocorrelator beams was blocked, leaving a single beam tightly focused onto the LED die. The average power of this beam was varied with the laser in both Pulsed and CW operation. Note that the chopper was still used to filter out any ambient noise. The results of this test are shown in Figure 17. The curve $y = 200x^2$is plotted with the data for comparison.

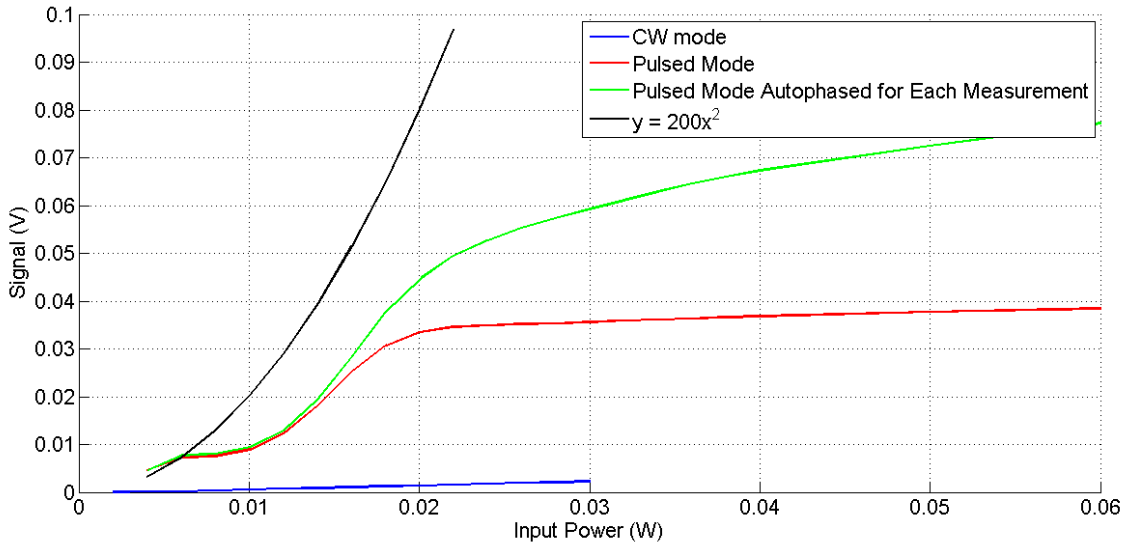

Figure 17: LED response

As expected, the nonlinear response gives no detectible contribution to the signal when the laser was operated in continuous-wave (CW) mode, and the response of the device is linear. When

pulsed operation was tested, the response of the LED was nonlinear even for the lowest obtainable power levels (in the range of 50 to 500 μW). However, a strange bend occurs in the response curve at approximately 6 mW. This is unlikely to be a measurement error as it is repeated in two separate sets of data. In addition to this anomaly, a clear saturation is observed when the average power exceeds 20 mW.

Additionally, a significant phase shift was noticed in the lock-in during these measurements. This is the same phase shift mentioned in Section 4.4. The overall phase shift over the entire range of measurement was approximately 60°, and is plotted in Figure 18. Because of this observation, two data sets were collected, one by leaving the lock-in amplifier's reference fixed and the other by re-referencing to the peak after each amplitude adjustment. Beyond about 15 mW this had a significant effect on the measured saturation level. However saturation still occurred at roughly the same average power in both data sets. It is interesting to note that the phase in a manner very similar to the shape of the signal response, and even saturates at the same point.

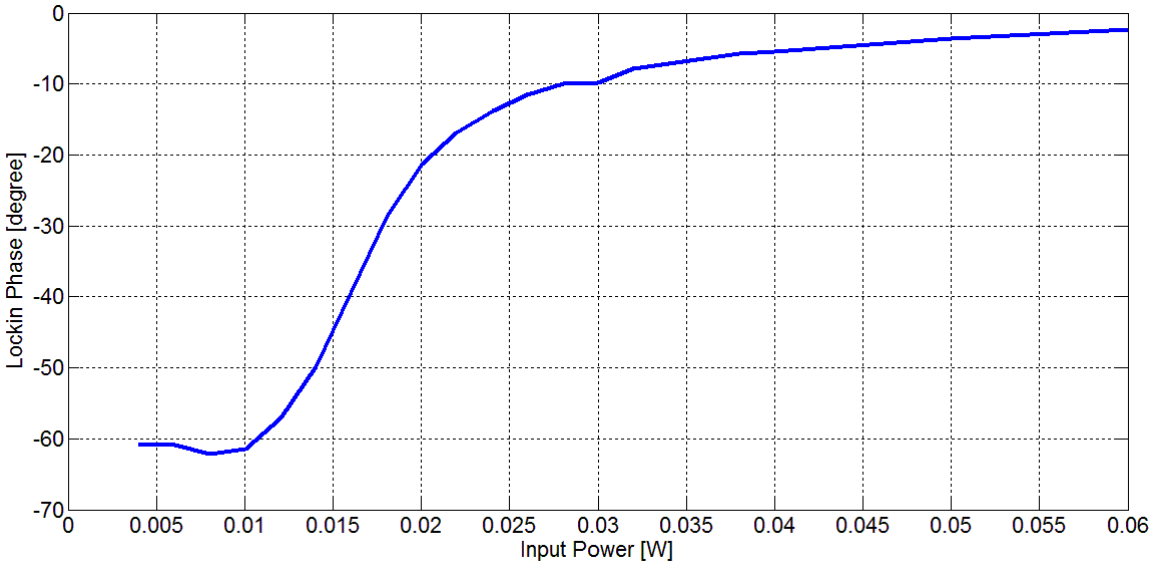

Figure 18: Lock-in autophase results vs. average input power

This relatively large shift cannot be an optical effect, since no components were moved during these measurements except for a rotation of the attenuators, which would not significantly change the focus or timing of the beam. The cause of this shift is difficult to determine. However, it is clear that something is shifting the phase of the carrier generation *measured by the lock-in* away from the phase reference of the chopper as power increases. The junction capacitance of the LED is a possible explanation for this. As the pulse power increases, more carriers, and hence larger currents, are produced in the LED. This is manifest through the lock-in input impedance ($R \approx 10$ M Ω) as increased recorded voltage. However, the increased number of carriers will take longer to discharge, resulting in an apparent phase shift that will be perceived by the lock-in, even though the chopper frequency and beam focus remain the same. This is consistent with the idea of the junction capacitance changing, and thereby increasing the measurement time constant. It is also consistent with the observed saturation. Once carrier production saturates, the decay time of the carriers can no longer increase, and no further phase shift would be observed. The change in capacitance dC necessary to produce the 60° phase shift observed above can be calculated. The chopper frequency was 377 Hz for all measurements. At this frequency, a 60°phase shift corresponds to a 442 μs shift in the measured signal. Using the standard formula for response time τ of an *RC* system gives:

$$\tau = RC \rightarrow \frac{d\tau}{dC} = R \rightarrow d\tau = RdC. \tag{8}$$

It can be assumed that the LEDs internal resistance is negligible compared to the 10 MΩ resistance of the lock-in amplifier. In this case, the necessary phase shift $d\tau$ = 442 μs requires a change in capacitance of 44.2 pF. This is a reasonable value for a diode, and provides a likely explanation for the strange behavior observed in the amplitude measurements discussed above.

4.6 Broadening Tests

After testing the response of the autocorrelation signals to varying input powers, an attempt was made to clarify the cause of broadening in the measurements. It was suspected that the observed broadening was due to the impulse response of the LEDs being larger than the FWHM of the laser pulses. To test this, a prism pair compensator was added to the output of the laser. The compensator is shown in Figure 19. The amount of dispersion was controlled by varying the distance between prisms, and this was used both to allow the laser to reach its minimum possible pulse width and to broaden the pulses.

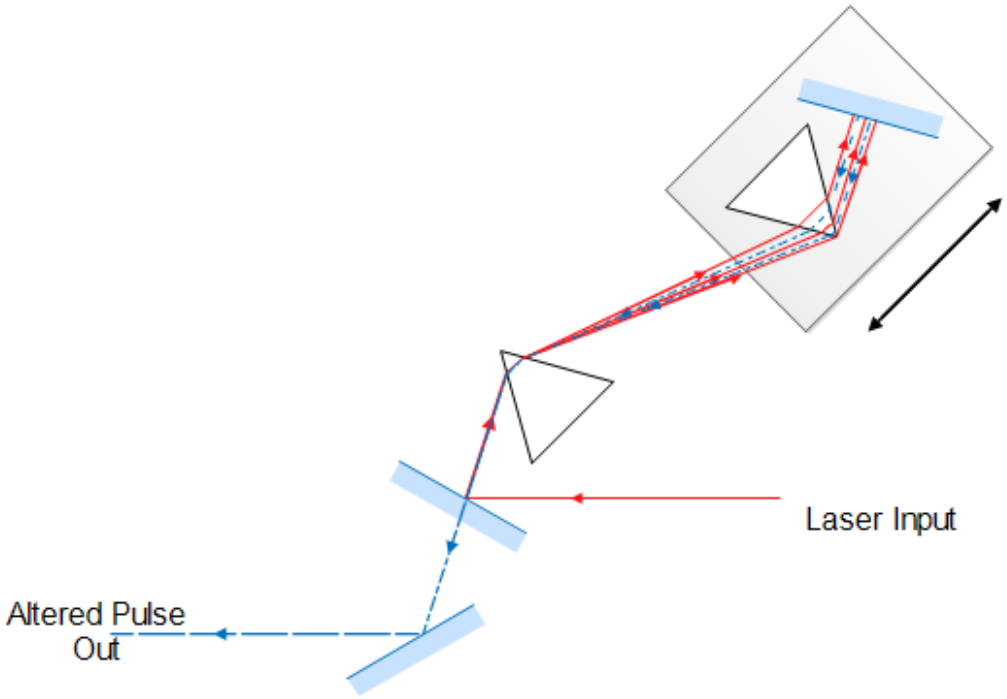

Figure 19: Compensator setup

Once again, control measurements were taken first with the BBO crystal autocorrelator setup. Autocorrelation measurements were made at a number of prism positions using the BBO crystal, creating measurements for a range of pulse widths. Several of these measurements are shown in

Figure 20. The shortest of these measurements had a FWHM value of 60 fs and the broadest had a FWHM value of 480 fs. These indicate actual pulse widths of 42 fs and 339 fs, respectively.

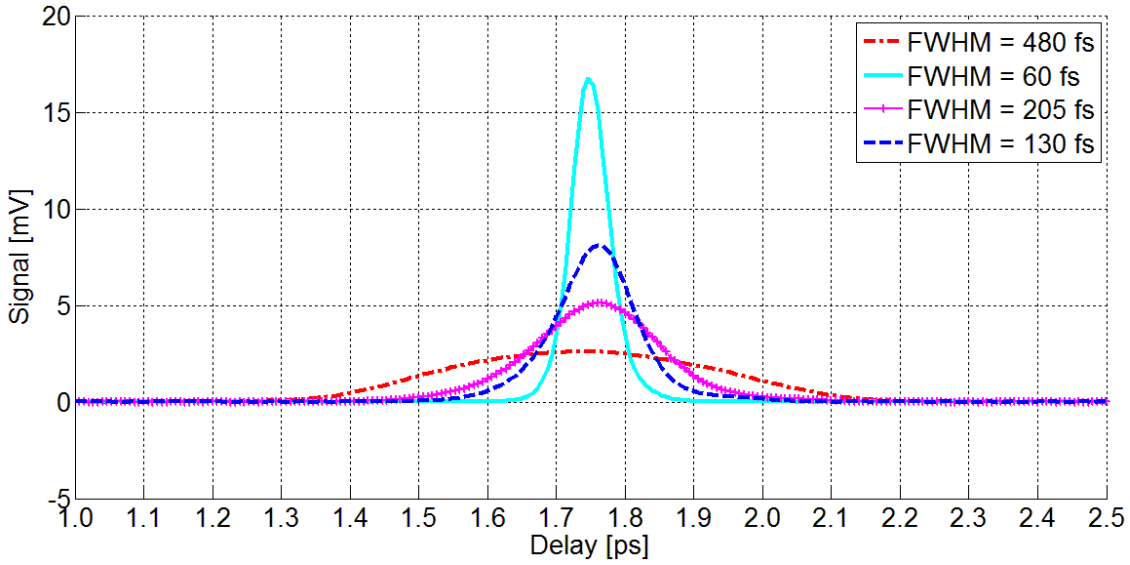

Figure 20: Broadened pulses measured with BBO crystal

The same measurements were then performed using the LED-based system with the amber LED. The peak intensity of the pulses was again reduced as the pulses broadened. However, the level of the signal floor also changed between measurements as in the previous experiments, causing difficulty in comparison. Therefore, the measurements were normalized and shifted to the same starting level for better comparison. This can be seen in Figure 21.

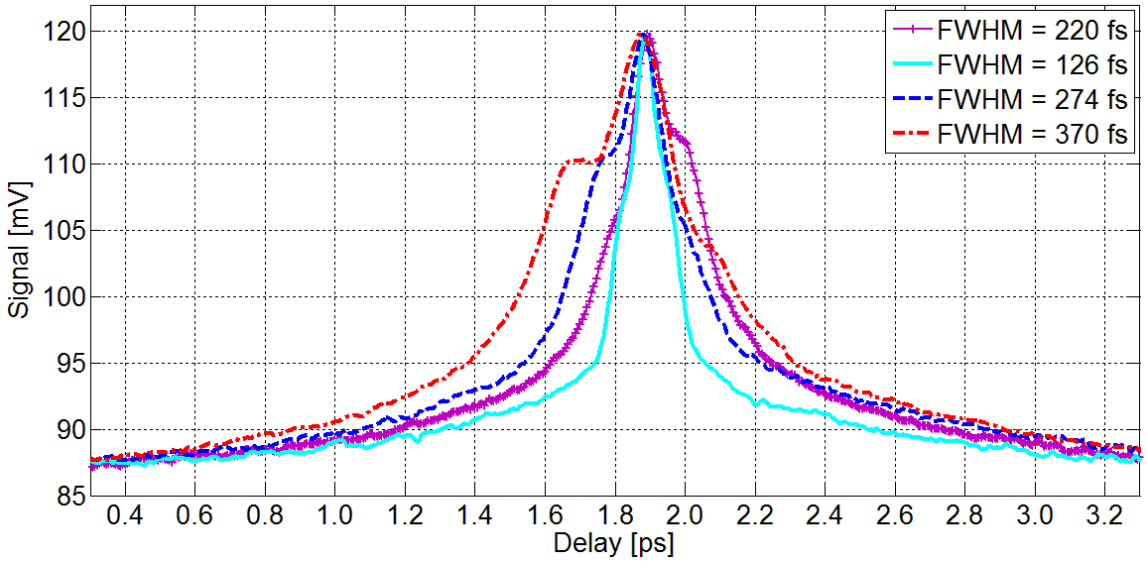

Figure 21: Broadened pulses measured with amber LED

These measurements display shoulders as before, but also have unusual indentations in the autocorrelation peaks. The asymmetric behavior of these features indicates that the order in which the pulses arrive now has an effect on the signal generated. This could indicate a misalignment in one of the beams, or interference from the wire bond on the LED die. Such an effect might not appear in the BBO-based autocorrelation measurements since the nonlinear crystal only transmits the overlapping components of the pulses to the detector. An alternative explanation can't be identified without further testing, and the features are considered to be the result of experimental error. After accounting for these unexpected features, the approximate FWHM of the LED measurements was determined (listed on figure). The FWHM changed with prism spacing as expected, resulting in measurements both broader and shorter than the original data set for the LED.

For clarity, the figures above do not show all of the measurements which were taken in this experiment. However, it is worthwhile to display the complete set of measurements for additional analysis. These are displayed in Figure 22 for both the BBO and LED-based measurements. The LED-based measurements are particularly interesting. The FWHM value of

these measurements decreases steadily as the laser pulses get shorter. However, the LED-based measurements appear to have a minimum FWHM value, as the last few measurements are nearly identical. This occurs in spite of the roughly equal change in prism spacing between measurements. This limit is not observed in the BBO crystal-based measurements, and indicates that there is a lower limit to the pulse widths that can be measured with LED-based devices. For our devices, this limit appears to be just above 120 fs. It is likely that various parameters of the photogenerated carriers, such as carrier lifetime, play a role in setting the minimum measurable FWHM value, at least for pulses on the order of 100 fs long. This theory is further supported by the fact that each LED in Section 4.2 reports a noticeably different FWHM value for the same 75 fs pulse, as it indicates that different doping and/or internal structure produces different levels of broadening.

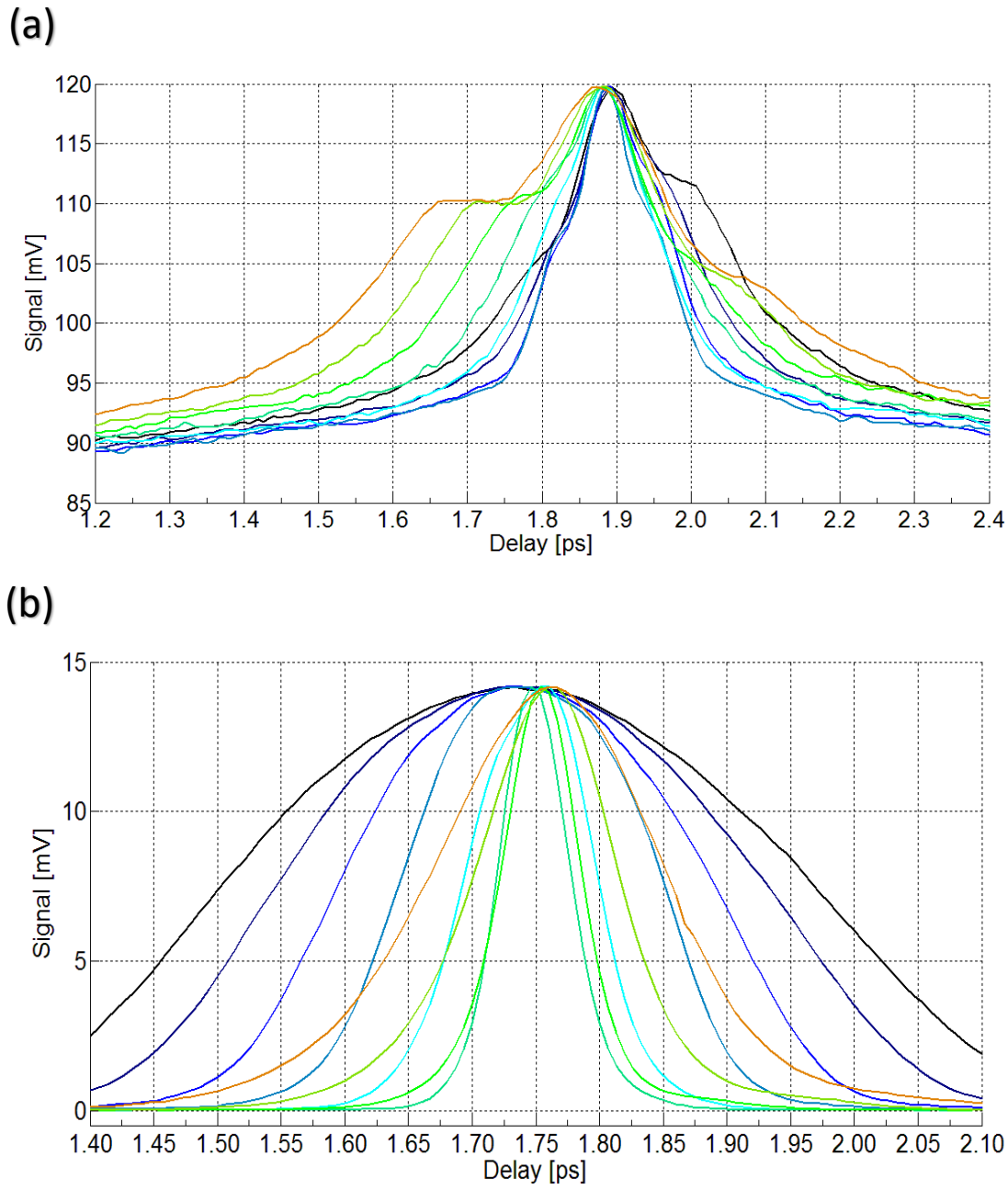

Figure 22: Normalized and zoomed plots (a) LED-based measurements and (b) BBO-based measurements with broadened pulses

4.7 Tests with Alternate LED

All of the previous testing revealed the same broadening features, but left unanswered questions as to why the broadening of the autocorrelation peak was occurring and why shoulders appear in the measurements. This stands out particularly since previous studies found no significant broadening. Broadening can come from various sources, such as group velocity dispersion, multiple reflections, and material effects. The remaining thin layer of epoxy on the LED dies was an unlikely but possible source of all these effects (see Figure 4(b)). The very small die combined with a relatively large gold wire bonded to the center may have also caused issues in measurement. To test this theory, additional measurements were performed with an OSRAM ultra-bright LED (model LE-A-QW9N), which also utilized an AlGaAs-based die. This LED has several advantages over the Cree LEDs used in previous measurements. The primary advantage being that the dies are much larger and are not encased in epoxy. Rather, the dies are shielded by a thin glass cover, which was easily removed. The OSRAM dies also have much larger active regions as shown in Figure 23, and these active regions are not blocked by the gold wire as in the Cree LEDs. This makes focusing of the laser pulses onto the die much easier.

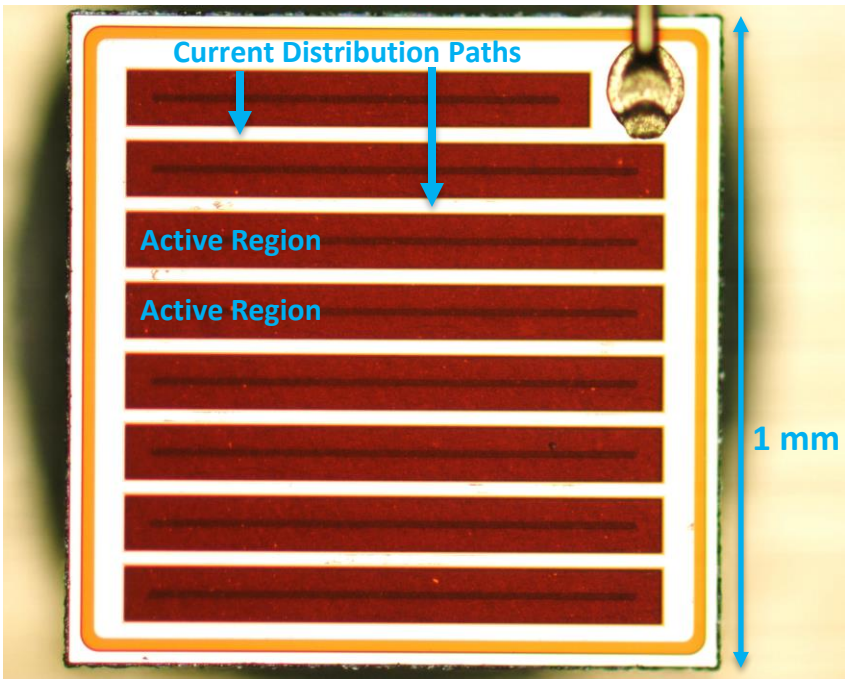

Figure 23: 10x Magnification of OSRAM LE-A-QW9N LED

Autocorrelation measurements were performed with these new OSRAM LEDs. The resulting trace is plotted in Figure 24.

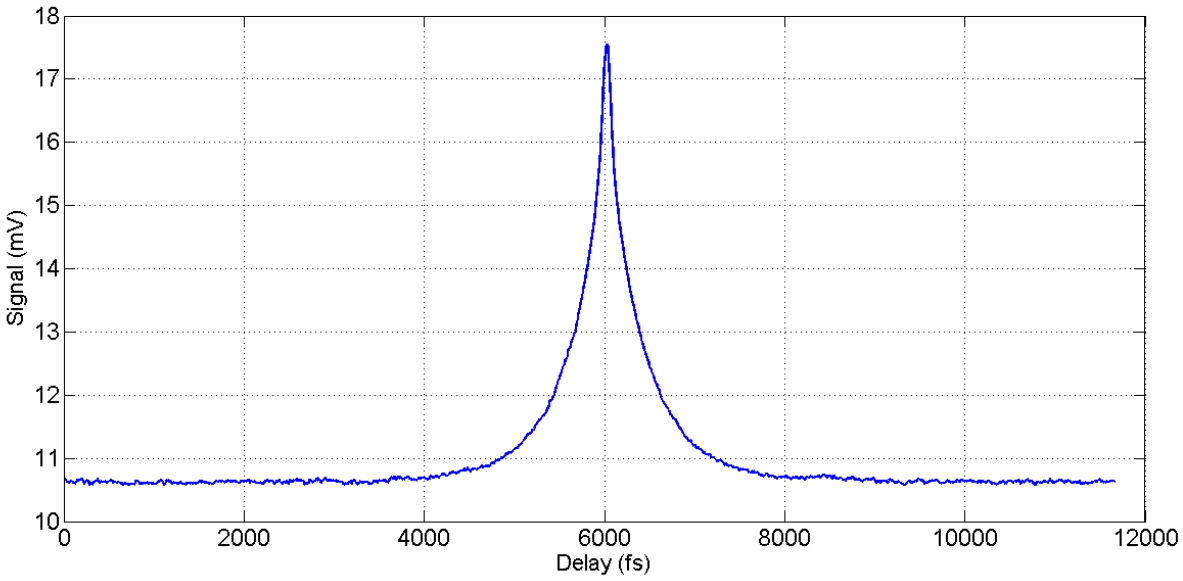

Figure 24: Autocorrelation measurement from OSRAM LED

The signal produced by these LEDs is considerably stronger. The LEDs still produce broadened autocorrelation measurements, showing a FWHM of approximately 150 fs . Note that this measuremet still has the same general features as those produced using the Cree LEDs . Namely, there is a strong sharp autocorrelation spike on top of smoother shoulders, although the distinction between the shoulder and autoccelation peak is much less obvious in these measurements. Several such measurements were collected to ensure the autocorrelation of Figure 24 was representative of the data. All of these measurements revealed the same basic shape and broadening. The most important aspect of these tests is the lack of encapsulant or covering on the die. This eleminates dispersive and multi-reflection effects as causes of the shoulders and broadening, showing that these effects must arise from a physical mechanism inside the diode. This mechanism could be either optical or electrical in nature, and will be discussed further below. The Osram measurements also eliminated the strange asymmetries in the data, suggesting further that some experimental artifiact due to the Cree LED's wire or the pulse width compensator caused them.

4.8 Discussion of Experiments

The experiments outlined above reveal several factors that must be explained. The first and most important is the broadened measurements and shoulders obtained when using LEDs. This broadening was observed in one photodiode study [7] but unreported in previous LED studies, possibly due to the much simpler PIN-type LEDs tested in many of those works. With technological progress over the last two to three decades, the drive for more efficient LEDs has rendered these PIN diodes obsolete, and it is all but certain that the LEDs tested in this work are of far more complex construction. There is also indication that there is a minimum measurable pulse width when using LED-based autocorrelators. These facts bode poorly for the use of LEDs as cheap alternatives to SHG crystals, especially since the effects appear to vary somewhat between devices. If LEDs are to be used as autocorrelation devices, the source of broadening and

the minimum measurable pulse width must be fully understood so that the actual pulse width can be accurately determined. If complete knowledge of the specific LED structure and detailed calculations are necessary, then LEDs become difficult for autocorrelation measurements, since this information is rarely freely available. The saturation discovered in the LED response may also play a role in this.

None of this implies that LEDs are without utility, however. Even if the FWHM value of the pulses cannot be accurately extracted, the very wide shoulders allow detection of pulse overlap at very large delays, and this concept can be very useful as a zero delay finder in a lab dealing with ultrafast pulses.

Finally, several important observations have been made with regards to the method of signal detection from the LEDs. While the signals generated in all tests were large enough to be measured by other means, it is apparent that the use of a lock-in amplifier is beneficial in LED-based autocorrelation systems. These amplifiers reduce noise and allow for more error in focus before the signal becomes impossible to detect. The placement of the chopper can have significant effect on the form of the signal, and the beam power and chopper position can be adjusted to reduce the signal floor to near-zero. As a practical benefit, many ultrafast laboratories are already equipped with lock-in amplifiers and time-delay steppers, meaning the addition of a very inexpensive LED enables such labs to perform high signal-to-noise autocorrelations, at least within the realm of the detectable time resolution.

CHAPTER V

Theoretical Studies

Several theoretical avenues were explored in an effort to understand the measured data. Simulation models were built mainly upon previous works involving carrier generation in semiconductors. There are many possible approaches, but they all require a nonlinear interaction to achieve the multiplication of signals that autocorrelations depend on. This limits the general approach to familiar mechanisms, such as 2PA and SHG. Any physical model must simulate carrier generation as its final output. This is because the measured signal is a current produced directly by the LED in response to the laser pulses. This current flows through the internal resistance of the lock-in amplifier to create the voltage measured in the experiments.

Of particular interest was determining the physical mechanisms which cause the autocorrelation broadening and shoulders in the measured data. As discussed above, these unique features in the experimental data are almost completely unreported in the literature and are never analyzed theoretically. Some work has been done to understand the source of the nonlinear response in LEDs and photodiodes. Authors have suggested that the autocorrelation measurements in LED detectors may arise not from 2PA, but rather from second-harmonic generation followed by single photon absorption, or from some combination of the two processes [5]. However, no experimentation or analysis has been performed to determine which is the case.

The purpose of these theoretical studies is to fill the gaps of understanding concerning carrier generation and detection when using LEDs in autocorrelation systems, and to explain the shoulders and broadening observed in our measurements. The well understood concepts of carrier generation, SHG, and other semiconductor effects are combined in a new model which attempts to achieve this goal. The ideal comprehensive model would include carrier transport effects in detail, but this necessitates a detailed knowledge of the LED physical structure, which was not possible in this work due to the secrecy on the part of LED manufacturers concerning device structure. Therefore, this section describes the work performed to achieve a more modest goal of describing various *possible* physical mechanisms that would produce the trends seen in the measured data. This has the very useful result of greatly narrowing the possible mechanisms at work, and may broaden understanding about how certain structures and material parameters affect the autocorrelation measurements of LEDs. The iterations of the simulation models as well as the necessary theory behind each is discussed below.

5.1 Eliminating Model Parameters

Since previous works have only speculated on whether 2PA or SHG is responsible for the autocorrelation signals seen from LED detectors, it is useful to attempt to rule out one or the other based on the measured data presented above.

The measured data suggests that SHG in the LED die is not responsible for the observed nonlinear response. This is mainly due to the fact that interference fringes are not observed in the measurements. As discussed above, the SHG which occurs in the BBO crystal produces a single beam of second harmonic light which travels to the detector and carries the autocorrelation signal. Any other signal components are redirected to miss the detector, as shown in *Figure 25*(a). However, when using an LED detector, both pulses are incident directly on the die. This means that *both* the SHG and absorption of the photons produced by SHG happen simultaneously inside

the die. Even if certain elements of the signal travel in different directions, they still produce carriers which would be detected by the amplifier. This is depicted in Figure 25 (b).

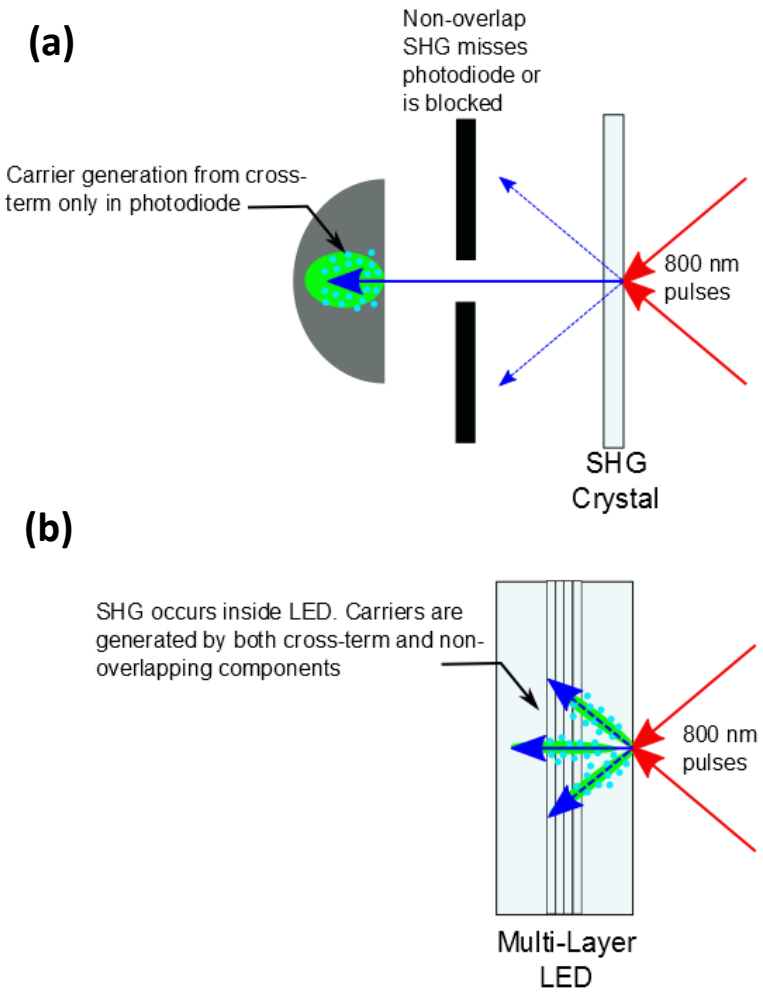

Figure 25: Carrier generation from SHG in (a) traditional autocorrelation setup with photodiode (b) LED detector

These extra signal components should also generate carriers, and the carrier generation would be given by the well-known form of the interferometric autocorrelation function [15]:

$$N(\tau) = \int_{-\infty}^{\infty} I^2(t) + I^2(t-\tau) + 2Re\{E^2(t)E^{*2}(t-\tau)\} + 4[I(t)+I(t-\tau)]Re\{E^2(t)E^{*2}(t-\tau)\} + 4I(t)I(t-\tau)dt. \quad (9)$$

This is the same form as found in an interferometric autocorrelator, where both pulses are sent collinearly to the detector, and this same mixing occurs. The extra terms arise from the field components which are normally redirected by the SHG crystal. An example autocorrelation trace from such a setup is shown below.

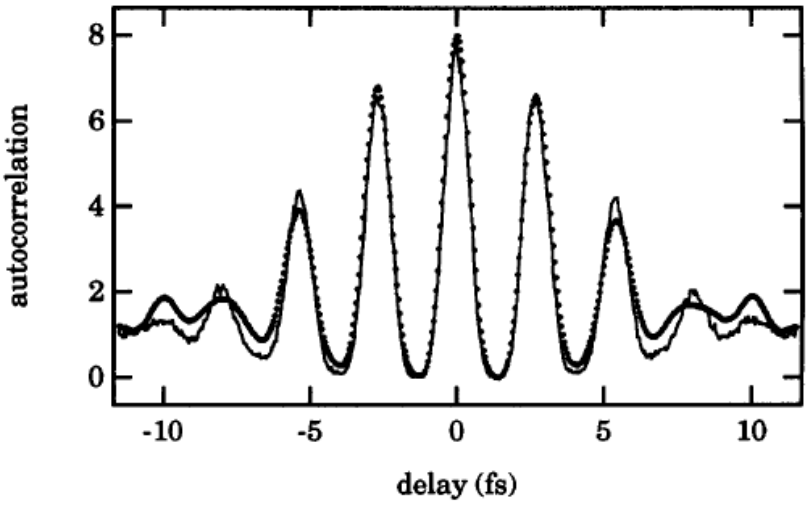

Figure 26: Sample interferometric autocorrelation trace [1]

The key feature observed in interferometric autocorrelations is the fringes superimposed on the main trace. Since the measured data from our experiments does not show these fringes, it is reasonable to assume that SHG is not the predominant mechanism of carrier generation. Note that this analysis is only valid if most of the carrier generation occurs at the focus of the two beams. Equation 9 is no longer valid once the beams spread apart. However, the analysis provides a sufficient starting assumption for the models. Therefore, the simulation models focus purely on 2PA processes.

5.2 Basic Carrier Generation Model

The first iteration of the simulation model was created to explore the effects of the one and two photon absorption coefficients on the final autocorrelation signal. For simplicity, the case

of a single slab of GaAs is considered. When the nonlinear two-photon absorption coefficient is considered, the formula for optical intensity vs depth becomes [8]:

$$\frac{dI}{dz} = -\alpha I - \beta I^2, \tag{10}$$

Where

α is the usual linear absorption coefficient [in cm^{-1}]

β is the two-photon absorption coefficient [in $\mathrm{cm/GW}$]

In addition, a given optical intensity will generate carriers according to a rate dependent on both single and two-photon contributions [8]:

$$\frac{dN}{dt} = \frac{\alpha I}{\hbar\omega} + \frac{\beta I^2}{2\hbar\omega}, \tag{11}$$

Where N represents the carrier generation in m^{-3}, ω is angular frequency of the light, and $\hbar$ is the familiar Dirac constant.

The analytic solution to Equation 10 is given by

$$I(z,t) = \frac{I(t)\exp(-\alpha z)}{1 + \beta I(t)\big(1 - \exp(-\alpha z)\big)/\alpha}. \tag{12}$$

Note that this reduces to the familiar $I(z,t) = I(t)\exp(-\alpha z)$ when no 2PA is present. This function describes the decaying optical intensity as it travels through a material. However, it is not useful alone. Equations 11 and 12 must be used together to determine the actual carrier density created. Using this physical modeling framework, a basic numerical simulation can be built that propagates the solution, step-wise, as the optical pulses travel through the slab of semiconductor. This simulation takes the following steps:

First, a value of delay τ is chosen by the simulation. The shape of the pulses at this value of τ is determined from the normal expression for Gaussian pulses given by Equation 6

Next, the slab of GaAs (or other material) is dived into layers in *z*, each layer having a width of *dz*. The resulting pulses are then input into Equation 12, providing a model of the propagation of the pulse in both time and space. This is visualized in Figure 27.

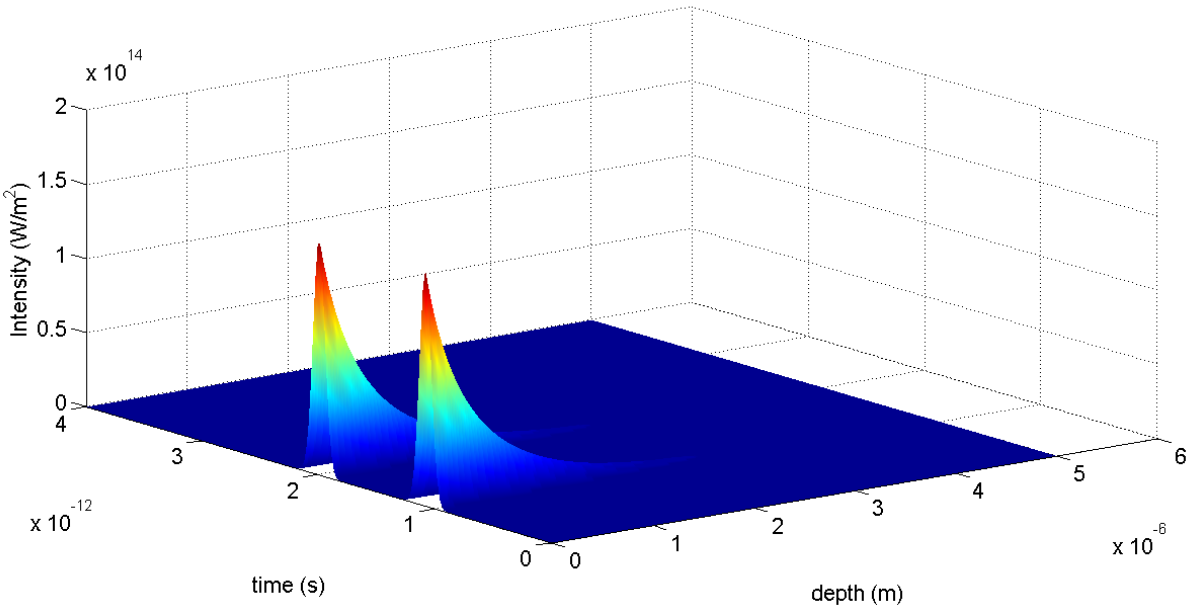

Figure 27: Simulated propagation of pulses in semiconductor slab

At each time *t*, there is a given intensity incident upon the GaAs slab. This is represented by the time axis in the figure above. Therefore, the original pulse shapes can be determined by viewing only this axis. For each value of time, the incident light propagates into the material, losing intensity according to Equation 12. The intensity at each point in time and space is recorded in matrix form by the simulation.

Next, the simulation takes the above intensity vs. space and time information and applies it to the carrier generation formula of Equation 11. The results are then integrated over time at each depth *z* to find the total density of carriers collected at that depth during the entire pulse event. Note that this is only valid because the entire event is assumed to happen much faster than the lifetime of the generated carriers and the detection time of the lock-in amplifier. This removes time

dependence from the data above, reducing it from three dimensions (time, depth, amplitude) to two dimensions (depth, carrier density).

Finally, the number of carriers at each depth is determined. The width of each layer in z is known from the simulation, and the area of the beams must be assumed. Then the total number of carriers generated at each depth is given by $n(z) = AN(z)dz$. The total number of carriers generated in the material is finally found by summing the number of carriers $n(z)$ generated in each layer.

The above process is repeated for every value of τ to construct the total autocorrelation signal. The result is a total number of carriers generated in the material by the two pulses for every value of τ, producing the autocorrelation function.

The model was tested with representative values for GaAs. The reported values of β vary from 0.07 to 23 $\mathrm{cm}^2/\mathrm{GW}$ [16], [8]. The purpose of these tests was to match the approximate behavior of the measured data. Therefore, a mid-range value of 10 $\beta = \mathrm{cm}^2/\mathrm{GW}$ was chosen. At 800 nm, the value of the absorption coefficient is approximately $\alpha = 10^4 \mathrm{cm}^{-1}$ [17]. The beam diameter was set to 10 μm, and the FWHM of the simulated pulse was 100 fs. The results from the model using these values are shown below:

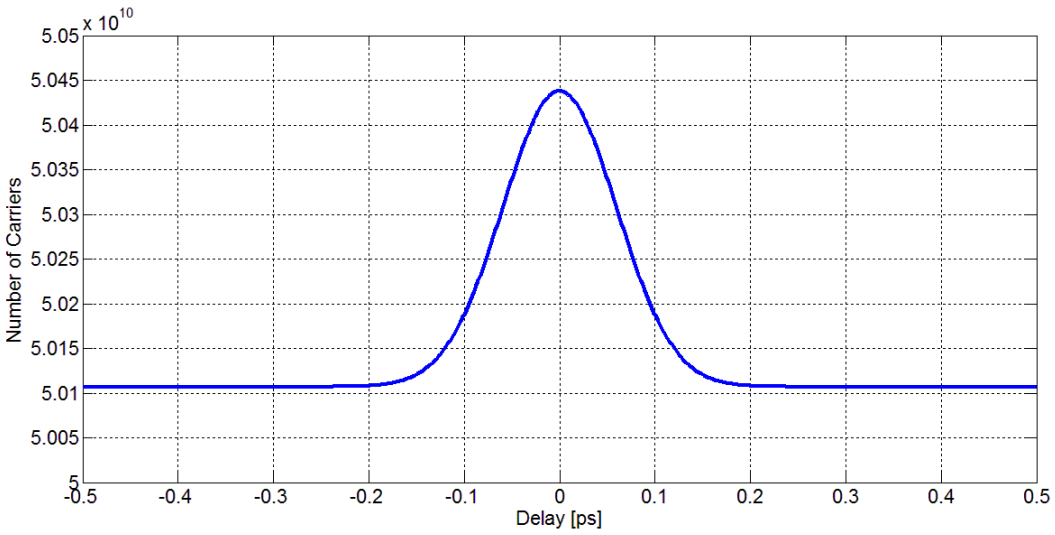

Figure 28: Basic model output

The output of the basic model behaves generally as expected, but does not match the measured data. As expected, the signal is offset from zero due to the fact that pulses always produce carriers in the material regardless of overlap. The number of carriers generated is also reasonable for a semiconductor material. However, the FWHM of the autocorrelation trace is approximately 140.5 fs, matching the expected factor of $\sqrt{2}$ increase from the pulse almost perfectly. The broadening seen in the measured data is not captured by this simulation. The signal shoulders are also absent. To explore the solution space of the simulation, the value of β was increased and decreased by up to two orders of magnitude. This altered the number of carriers in the autocorrelation, but had no effect on the FWHM value of the generated autocorrelation trace. The values of α were varied in the same way, and also did not change the FWHM value of the simulated trace. No modification to the model parameters resulted in the broadening or shoulders observed in the measured data. These tests show that, while the basic model behaves as expected, it is missing a fundamental mechanism and cannot recreate the measured data.

5.3 Addition of Free Carrier Absorption Mechanism

The process of free carrier absorption (FCA) was considered as a possible mechanism for the broadening of pulses. This mechanism describes the process in which free carriers generated by single or two photon absorption absorb additional photons [18], [19], [20]. The effects of FCA can be thought of analogously to saturable absorption. Saturable absorption in general is a well-known phenomenon often used to shorten ultrafast pulses in transmission by strongly absorbing the weak intensity in the pulse tail that follows the strong peak. In our experiments, FCA should be expected to cause the opposite effect. This is because the autocorrelation is not dependent on transmission of light through the LED, but instead on generation of carriers in the LED. Every photon that is absorbed by FCA is now unavailable to produce a new detectable carrier. In this case, the low-intensity leading edge of the pulse should produce few carriers, and be unaffected by FCA. As the pulse intensity increases, many more carriers are generated, and FCA from these carriers will begin to block the optical pulse from producing more. This effect would be even more extreme when the two pulses overlap and further increase the total intensity. Therefore, FCA processes could be expected to reduce the *peaks* of the autocorrelation function and leave the signal tails relatively unchanged. This would have the effect increasing the apparent FWHM values of the autocorrelation measurements.

To test this theory, the simulation model was altered to include the effects of FCA. When these effects are included, the formula for intensity becomes [8]

$$\frac{dI}{dz} = -\alpha I - \beta I^2 - \sigma_{ex} N I, \tag{13}$$

where σ_{ex} is the FCA coefficient in cm^{-3} and the carrier density is given by Equation 11 as before.

Unfortunately, the set of differential equations consisting of Equations 11 and 13 can no longer be solved analytically once the FCA term $\sigma_{ex}NI$ is added to the intensity [8]. The simulation model must be changed to find the solution entirely numerically. To do this, the detector material is broken into layers of very small thickness *dz* as before. The initial value of *N* is assumed to be zero in all layers. The simulation starts with the first layer of the material and the optical pulses are applied to this layer, evaluating Equation 13 for the given layer only at every value of *t*. At each value of *t*, the intensity at the back side of the layer is evaluated as $I_{next}(t) = I(t) - dI(t)$, where $I(t) - I_{next}(t)$ is very small due to the small *dz*. The resulting value of $I_{next}(t)$ is used to determine $\frac{dN}{dt}$, and this is used along with the knowledge of the value of *dt* to determine the change in carrier density produced during that time step. This process is repeated for all values of *t* over the entire pulse event. When finished, the total carrier density *N*(*z*) is known for the layer in question. The complete post-layer signal $I_{next}(t)$ is also known. This process is repeated for the next layer, using $I_{next}(t)$ as the new incident intensity upon the next layer, and the process continues for all subsequent layers of the device.

The simulation method outlined above produces the total carrier density generated in each layer *dz* as before. The assumed beam area and value of *dz* are once again used to convert this information into the total number of carriers per layer, and these numbers are added to determine the total number of carriers generated in the LED over the entire pulse event. This process is repeated for each value of *τ*, resulting in an autocorrelation trace as before.

To test the new model, the value of σ_{ex} was set to zero and the resulting intensity decay in *z* was compared against the previous analytical solution. Good agreement was found between the model and this solution. Next, and before performing autocorrelation simulations, the general response of the model was tested. This was done by inputting a single Gaussian pulse of varying average powers into the model and observing the output. This resulted in a significant decrease in

the number of generated carriers for the data shown and a new saturated shape to the response. Note that the value of α was effectively reduced to zero in order to isolate the effects of the FCA cross section. The simulation was first tested without FCA effects enabled ($\sigma_{ex} = 0$). This is shown in Figure 29(a), and was done to confirm that the new simulation model displayed the expected nonlinear response to increasing average beam power. Next the effects of FCA were added to the model by setting σ_{ex} to a nonzero value. The result of this test is shown in Figure 29(b).

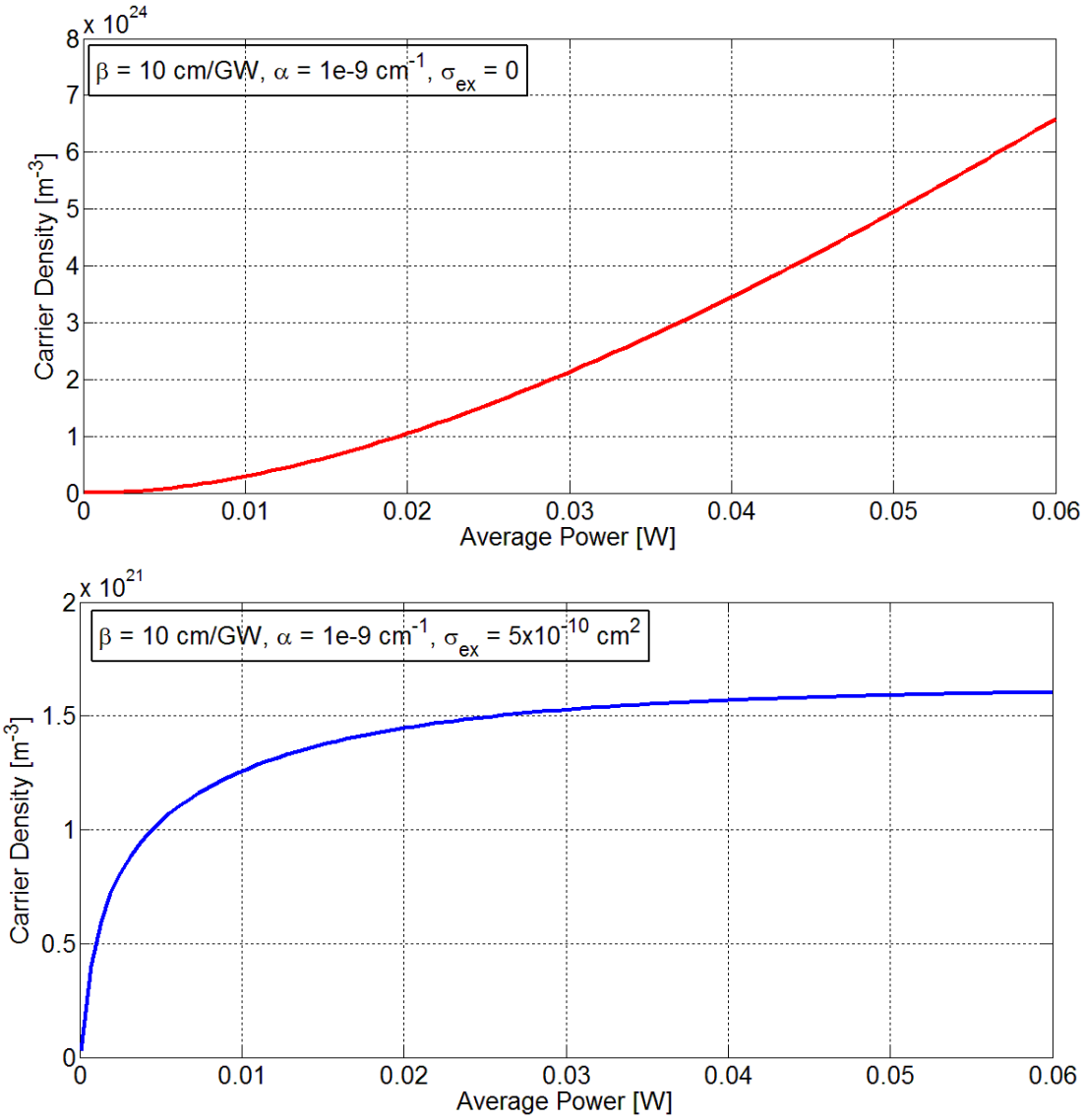

Figure 29: Simulated response to varying average beam power (a) without FCA effects (b) with strong FCA effects

These tests show partial agreement with the measured data (in Figure 17). When FCA effects are left out of the model, the response is purely nonlinear and increases without limit as the average power rises. Adding FCA effects to the model breaks this trend and causes saturation behavior as expected. The best match to the trends seen in the experimental data was achieved with free carrier cross sections of $\sigma_{ex} = 5 \times 10^{-10}$ cm^2. These simulations do not match the measured data perfectly, but do show the expected saturation. The large value of σ_{ex} required to obtain this

behavior is more concerning. This is a much larger value than is typically reported in the literature for pure GaAs [19], [18]. It is therefore likely that FCA is not the only mechanism at work to cause the observed saturation. Another possibility is that the maximum carrier density is being reached when saturation occurs. This cannot be confirmed without greater knowledge of the LED composition. Finally, note that the number of generated carriers is not unreasonably large, and has been considerably reduced by FCA, as expected.

Autocorrelation simulations were performed next with these values of σ_{ex} to determine whether FCA could contribute to the observed broadening. The results of these tests are shown in Figure 30. Note that the simulated traces for $\sigma_{ex} = 0, 1 \times 10^{-16}$, and 1×10^{-14} cm^2 are effectively identical. Also note that a detectable autocorrelation trace exists for $\sigma_{ex} = 1 \times 10^{-10}$ cm^2, but its amplitude is low enough to appear as zero in the figure. This trace was multiplied by a factor of 300 and shifted (green dot-dashed line) for better comparison with the other simulated traces. Values larger than $\sigma_{ex} = 1 \times 10^{-10}$ cm^2 produced effectively zero amplitude signals, since this value is so large that almost all of the pulse is immediately absorbed.

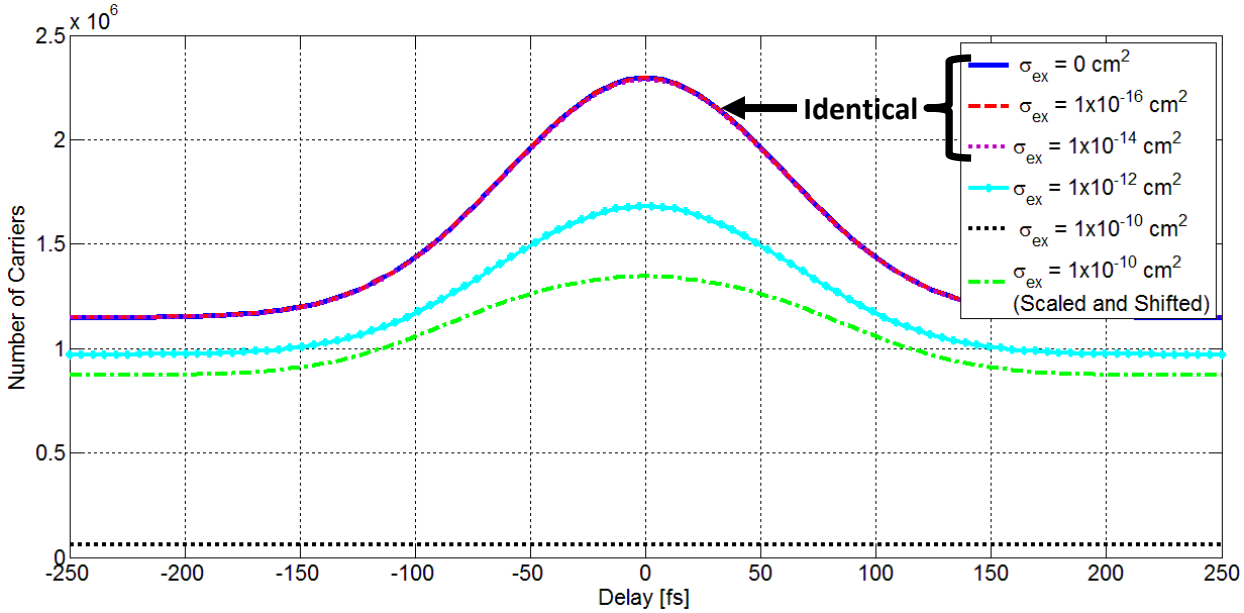

Figure 30: Simulated autocorrelation measurements with various FCA cross sections

No broadening was achieved in the simulation for FCA cross sections smaller than 1×10^{-14} cm^2. The cross section $\sigma_{ex} = 1 \times 10^{-16}$ cm^2 produced a FWHM of only 150 fs, which is a negligible increase from the theoretically expected 141 fs. Only a modest broadening was observed even with the extreme and unrealistic FCA cross sections $\sigma_{ex} = 1 \times 10^{-10}$ cm^2, which gave a FWHM value of only 176.8 fs. These simulations further confirm that FCA is unlikely to be the sole cause of the broadening observed in the measured data. The extremely large values of σ_{ex} required to produce *any* broadening and the very small increase in FWHM even at these large values are both indicators of this.

This is an undesirable result, but it can be explained by analysis of the nature of the Gaussian pulses. The original assumption was that FCA may attenuate the peak of the autocorrelation signal, making the trace appear broader. However, while the peak *can* be reduced, and was, the base of the signal can never be widened by this mechanism. That is, the signal tails never spread beyond their original temporal extent. This means that, even if the peak reduction is extreme to a physically unreal extent, the FWHM of the autocorrelation can never be broadened beyond the width of its original base, which was about 300-400 fs in simulations above (note that width of the autocorrelation base is approximately 800 fs in the measured data of Figure 8). Any further reduction in the peak would simply eliminate the signal. In more physically realistic simulations, the broadening is even further limited, because FCA is clearly not the dominant mechanism. From these simulations, it was concluded that FCA probably plays a role in the observed saturation seen in the measurements of Figure 17, but it is very unlikely to account for the broadening observed in the measured autocorrelations. In addition, FCA did not produce the shoulders observed on the measured signals.

5.4 Carrier Decay and Collection

Until this point, all previous versions of the simulation model had assumed an infinite carrier lifetime. This assumption is valid as long as the photogenerated carriers have a lifetime much longer than the entire two-pulse event (in the range of hundreds of picoseconds to nanoseconds). Under this assumption, every carrier generated over the duration of the two optical pulses can be considered to be a part of the autocorrelation signal. Here it is assumed that all photo-generated carriers would eventually find their way to the device contacts and into the lock-in amplifier. However, it is certainly possible for carriers to have a sub-nanosecond lifetime, depending on the device materials, their layering, and their growth quality. For example, sub-picosecond lifetimes in GaAs based alloys have been deliberately engineered by such techniques [21]. Moreover, a device which is designed to emit light would be expected to have a minimized carrier lifetime in order to promote instant radiative decay.

The inclusion of carrier decay in the model does not only serve to make the simulation more physically accurate. It also provides a partial answer to the cause of shoulders in the measured data. When considering the nature of autocorrelation traces, it becomes evident that *any* signal above the floor of the trace must be due to the interaction of the pulses. The existence of these shoulders show that the pulses are finding some way to interact at larger delays than expected, producing shoulder signals that appear well beyond the extent of the original pulse overlap. This cannot be caused by an optical mechanism in the LED die. The LED dies are too thin for internal reflections to cause interactions at such large delays, and broadening has been ruled out by the fact that these shoulders persist even with the bare OSRAM dies. Dispersion inside the dies is also extremely unlikely. This is because, according to the well known Kramers-Kronig relations, significant dispersion must be accompanied by significant absorption. Therefore, large absorption at 800 nm would be required to cause dispersion in the LED dies. Since these dies are designed to emit in the amber and red spectrum, it is highly unlikely that they

possess large absorption at a wavelength so close to their intended emission wavelength. Therefore it is clear that some other mechanism is required which allows the effects of the first optical pulses to linger long enough to interact with the second pulse. Photo-generated carriers are able to do that, however their lifetime cannot be very long in that case, since it would imply that autocorrelation signals would have measurable components over very large time spans, longer than that observed in the measured data.

Note that double-pulses and other instabilities have been known to cause similar shoulders in traditional intensity autocorrelators [22]. However, this possibility has been ruled out by several factors. First, the laser spectrum remained stable during all experiments. This does not indicate conditions which could cause significant double pulses. Additionally, glass in the system was minimized, making double pulses from reflections unlikely. Finally, the strongest case against this theory is the fact that no shoulders were seen in any SHG control measurements using the BBO crystal. These measurements were performed after every major adjustment to the system, and never showed shoulders or other issues. These facts point to an effect unique to the LEDs, and this effect must be electrical in nature.

The shape of the autocorrelation signals also provides clues about the nature of this interaction. Their exponential appearance in the measured data appear quite similar to that observed in optical pump probe measurements of materials with relatively short carrier lifetimes, on the order of a few picoseconds.

For these reasons, a carrier decay and linear interaction mechanism were added to the simulation model. This alters the formula for carrier density to the following:

$$\frac{dN}{dt} = \frac{\alpha I}{\hbar w} + \frac{\beta I^2}{2\hbar w} - \frac{N}{\tau_c} - \frac{N}{\tau_{rc}} + LNI. \tag{14}$$

The carriers which reach the amplifier and produce a signal are now modeled by the following formula:

$$\frac{dN_{collected}}{dt} = \frac{N}{\tau_c}. \tag{15}$$

This formula has several new terms which must be described in detail. In this new formula τ_c represents the carrier collection lifetime, in seconds. This value determines the rate at which carriers are collected by the amplifier. Only the carriers which are collected are considered to be part of the autocorrelation signal. Similarly, τ_{rc} represents the rate at which carriers recombine naturally in the LED. Note that τ_c and τ_{rc} together represent the total decay of carriers in the LED. They are separated into two terms because of the very different effects that each process has on the measured signal. Recombined carriers reduce the number of carriers present in the device at any given moment, but are not "collected" amplifier. They are permanently lost and do not become part of the autocorrelation signal. Conversely, only carriers that "decay" into the amplifier produce any signal. This is not strictly a decay process, but the mathematical form of the collection is the same. Finally, the parameter *L* is a fitting parameter represents an additional linear response to the carrier concentration.

The linear parameter *L* is important and requires a bit of discussion. Recall that the appearance of shoulders was speculated to be due to the second optical pulse interacting with carriers produced by the first. So long as this interaction is possible, and photo-generated carriers have a modest lifetime (1-5 ps), the second pulse can produce an autocorrelation signal with shoulders extending to time scales of the same order. The linear term was born from the indication that the second pulse must be interacting with the carriers left over from the first. It is a linear term similar to α, based on single-photon interactions. However, it is not only dependent on the optical intensity, but also on the number of carriers present in the device at a given time. So long as carriers are present from the first pulse (captured in the value *N*), the intensity from the second pulse

(captured in *I*) will produce additional carriers. These additional carriers will be manifest in the signal measured on the lock-in through the term N / τ_c.

Using this new model, the following results were obtained:

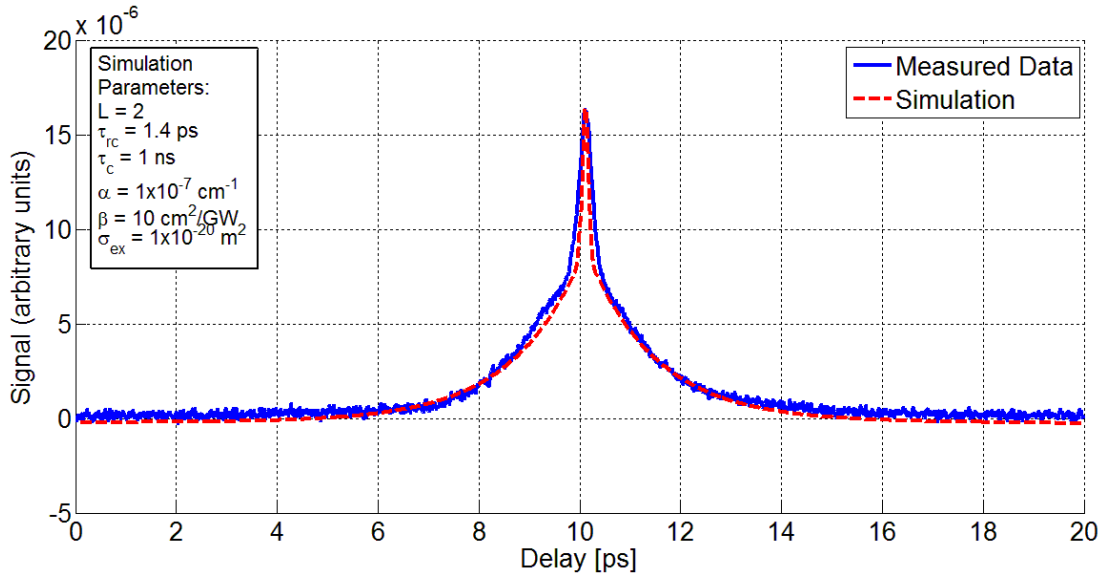

Figure 31: Simulation result in agreement with Cree data

This autocorrelation trace shows excellent agreement with the measured data from the Cree amber LED (in Figure 15 and Figure 16 for example), particularly in the shoulder behavior. The FWHM of the simulated autocorrelation peak (with an approximate value of 160 fs) does display *some* broadening, but this aspect of the simulation does not match the data ideally. It is worth noting some other performance characteristics of the simulation. As expected, τ_{rc} and τ_c are interchangeable without altering the trends in the simulated autocorrelation trace. The number of carriers collected is obviously changed, but the FWHM and relative amplitudes of all features remain the same. Again, this is because the *total* loss of carriers (represented by both terms) is responsible for the shoulder shape. A final and very important confirmation is the dependence on the linear factor *L*. If this factor is set to zero, both the broadening and the shoulders vanish from the simulation as expected.

Increasing the linear factor *L* to 3 increases the shoulder height. This increase combined with an adjustment of the carrier lifetimes produces a simulation result in very good agreement with measurements from the OSRAM LED. This is shown in Figure 32.

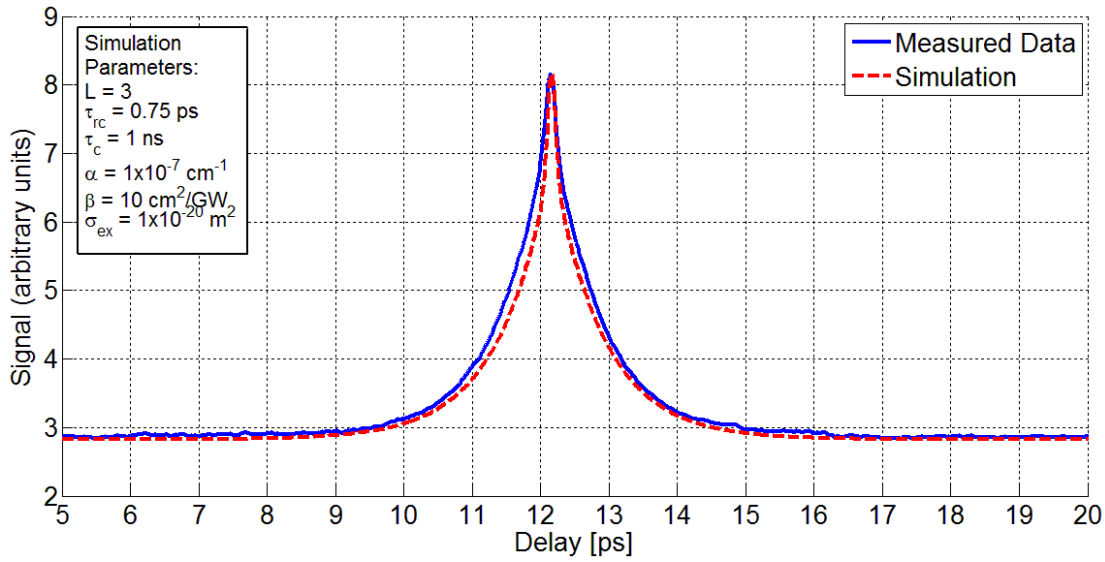

Figure 32: Simulation results in agreement with OSRAM data

Again, the shoulder behavior is matched extremely accurately, while the signal broadening is not captured by the simulation. Several important factors can be understood from these simulations. First, the dependence of shoulder width on recombination times suggests that the full extent of shoulders is due, in part, to recombination of photogenerated carriers produced in the LED. The autocorrelation picks up these carriers as they decay in a similar fashion to pump-probe measurements, producing the shoulders seen in the measured data.

Both the shoulders and broadening were found to be highly dependent on the linear factor *L* in the simulations. Additionally, the shoulder behavior from the experimental data of multiple LEDs was able to be precisely matched by adjusting this parameter. These facts help to confirm the legitimacy of this model and the linear interaction. However, this does not provide any information on the specific cause of this interaction. The question is what kind of physical mechanism could cause carrier production dependent on the signal intensity (*I*) and the number of

carriers already present (*N*). As discussed, this is the only way that a second pulse could create an autocorrelation signal when the first pulse has long since exited the system. It is here that the full knowledge of the LED material structure would be extremely valuable. The model presented above cannot determine what specific physical process is responsible for this, but several known mechanisms could be responsible. These are discussed below.

As mentioned previously, modern LED design has evolved significantly from the simple PIN diode. In modern LEDs it is not uncommon to find a quantum well, or multi-quantum well structuring. In fact, devices without such structure are no longer likely to be manufactured for general sale. The motivation behind this is plural. Manufacturers seek not only to produce specific wavelengths, but also to maximize the efficiency of energy conversion in the diodes. In part, quantum wells tune the radiative bandgap, and thereby help to produce the correct wavelengths of light. Quantum wells also serve to rapidly capture injected carriers forcing them to decay radiatively. As stated before, the structure can also serve to tune (i.e. shorten) carrier lifetime, which is beneficial in radiative devices. However, there can be numerous energy levels within quantum wells, and these can interact differently when high-power optical pulses are involved. Therefore, these quantum well provide a possible mechanism that may account for the linear term *L*. Carriers, generated by an optical pulse, can relax into the wells just as if they were electronically injected. It is then possible that these carriers may be promoted back out of the well by a following optical pulse. If the well depth and internal energy levels are such that this promotion energy is below that of a single photon energy of the optical pulse, then the promotion is highly probable. In this case, the response of the LED to a pulse would be much stronger if a previous pulse had passed through within the lifetime of these carriers. Such a mechanism would be manifest by the linear term in Equation 14.

Other mechanisms may also be possible and would exhibit the same sort of re-promotion of carriers into a free-conduction state. Indeed, any kind of semiconductor trap, wherein selection

rules permitted re-promotion, would enable the linear term in Equation 14. This could come from either intentional structure or material defects. Modern LEDs have quite complex semiconductor structuring that could permit this mechanism in a number of ways.

The critical point to note is that some mechanism must permit carriers to interact with a following optical pulse on the order of picoseconds after the first pulse as exited. No other effect can reproduce the experimental results. This is likely to be a linear interaction. This interaction must also result in measurable current, or its effects would not be present in the measured data. This requires that the responsible mechanism involve interaction with carriers, and suggests a re-promotion of carriers to free-conduction as the likely candidate. Moreover, the linear term in Equation 14 produces simulation results that are very similar in functional shape and detailed amplitude and temporal qualities to the experimental results. While the lack of LED structural details prevents any determination with full certainty, the result shown here strongly suggest a general mechanism at work.

5.5 Varying Pulse Width

After obtaining a reasonable simulation model, the FWHM values of the simulated pulses were varied. This was done to test whether the carrier lifetime and collection mechanisms presented in the model above would replicate the behavior observed in section 4.6. In this case, the FWHM value of the simulated autocorrelation traces should also have a minimum. Further reducing the simulated pulse widths below this minimum should not significantly alter the resulting autocorrelation trace. The results of these tests are shown in Figure 33.

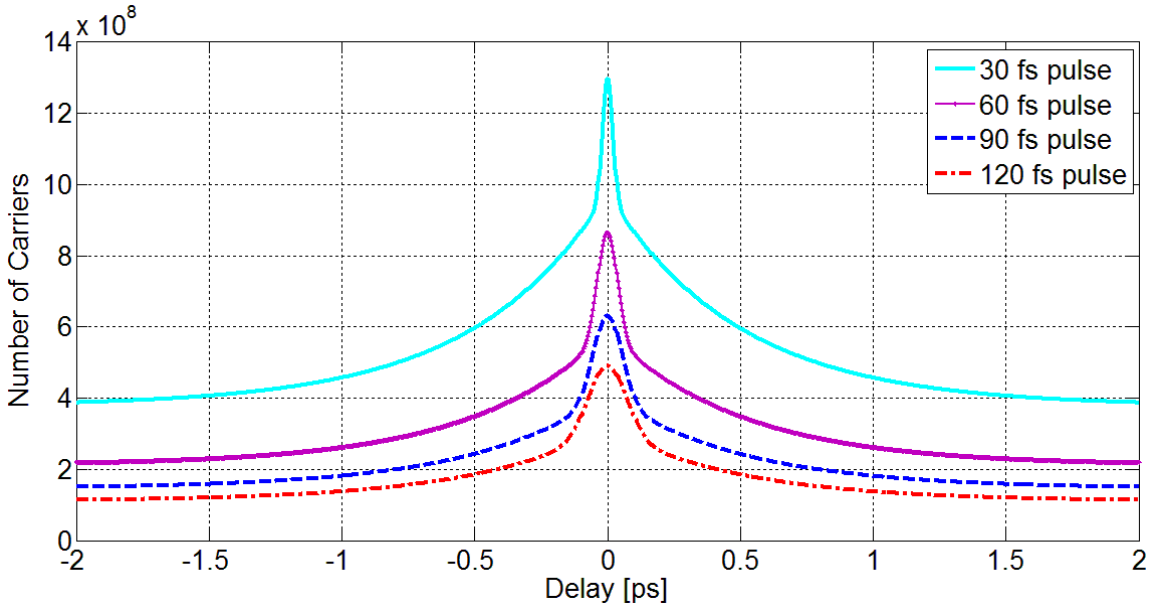

Figure 33: Simulated autocorrelations for various pulse widths

Unfortunately no lower limit on the FWHM value was found in the simulation model. This suggests that a mechanism not included in the model sets the minimum measurable FWHM value. This mechanism could involve broadening of the optical pulses due to dispersion or other effects internal to the LED die, but further experimentation is needed to identify the exact cause.

5.6 Discussion of Simulations

The simulations above have been successful both in eliminating physical mechanisms that cannot contribute the observations made in the measured data and in identifying potential mechanisms that could be at work. The broadening of the autocorrelation traces was not fully captured in the simulation models, and recommendations to reduce this effect cannot be made. However, the other trends in the measured data have been matched with good agreement. Second harmonic generation followed by absorption has been ruled out as a mechanism by which the LEDs produce any nonlinear signal, and the likelihood of 2PA as the dominant nonlinear mechanism has been shown. It has also been shown that FCA is not a contributor to the broadening and shoulders seen in the measured data, however it may play a role in the saturation

behavior observed. Finally, finite carrier lifetimes via recombination, along with carrier re-promotion to the conduction band, have been demonstrated as very viable candidates for the cause of the shoulders observed in autocorrelation measurements. From these findings, it can be seen that when using LEDs as a zero-finding tool in ultrafast setups, devices with the longest possible carrier lifetime should be chosen to lengthen the shoulders and aid in detection of the signal. This would also aid in signal detection even in cases where the system is used purely as an autocorrelator.

CHAPTER VI

Conclusion

The goal of this research has been to explore the performance of LED-based autocorrelators and to more accurately characterize the response of these devices. In pursuit of these goals, a number of useful insights have been gained, and potential alternative uses for these effects have been identified.

The numerous experiments which have been performed show a fundamental shift in the performance of modern-day LEDs when used in autocorrelation setups. Signal shoulders and large broadening are now common. This coincides with the increase in the complexity of this technology since LED-based autocorrelation experiments were last reported in the literature. Dispersion and other optical effects have been ruled out as candidates for these effects, and a likely electrical mechanism has been identified. Carriers which remain present in the LED die after the first pulse have been shown to interact with the delayed second pulse from the autocorrelation system. The lifetime of these carriers is long in comparison to the duration of the pulses, and this allows the two pulses to effectively interact across a much longer range of delays than would be expected from a standard autocorrelator. This mechanism strongly influences the width and shape of the signal shoulders, and can be minimized with very fast

recombination of carriers in the LED die. However, the choice of these parameters is not possible when selecting commercial LEDs for use in an autocorrelation setup. In fact, it is often impossible to even obtain the necessary information to *determine* these parameters for a given LED. This poses a problem for those desiring to use LEDs in autocorrelation systems, however, it also presents an opportunity for alternate uses.

While it may not be practical to use commercial LEDs as femtosecond autocorrelation detectors, the devices have many features that make them extremely useful in an ultrafast laboratory. First, they can still likely be used for picosecond pulse characterization. Second, they are significantly easier to focus than common SHG crystals, and they provide real-time feedback on the quality of focus. Third, the autocorrelation traces produced by these devices exhibit wide shoulders with a pronounced peak at the center, making their location in time extremely easy to identify on long scan pump-probe type systems. The picosecond extent of the shoulders allows vary large steps (on the order of hundreds of micrometers) to be made during the scan without missing the signal. This is in contrast to a 100 fs autocorrelation with no shoulders (as produced by traditional SHG-based methods), which can easily be missed entirely during a zero-finding measurement by simply jogging the stepper a few microns too far. Finally, they offer an extremely large range of detection and strong output signal (on the order of 100 mV), making them even more useful in the determination of zero-delay in optical systems, with minimal setup time. The necessary setup can be constructed with very low cost and little time, eliminating the need to align an experiment *before* zero delay can be confirmed. All of these features make LED-based autocorrelation an extremely useful technique in finding zero delay, although it may be lacking for actual determination of FWHM pulse values.

REFERENCES

[1] J. K. Ranka and A. L. Gaeta, "Autocorrelation measurement of 6-fs pulses based on the two-photon-induced photocurrent in a GaAsP photodiode," *Optics Letters,* 1997.

[2] S. A. Aljunid, "Optical Autocorrelation using Non-Linearity in a Simple Photodiode," National University of Singapore Department of Physics, 2007.

[3] J.-H. Lei, J.-S. Chang, Y.-C. Noh, "Visible wavelength antocorrelation based on the two-photon absorption in a SiC photodiode and a GaInN light emitting diode," in *The Pacific Rim Conference on Lasers and Electro-Optics*, 1999.

[4] N. Kurahashi, N. Kagawa, T. Matsuyama, K. Wada, H. Horinaka and Y. Cho, "Real-time intensity and phase-fringe ultrafastoptical pulse antocorrelator based on a two photon absorption of a light-emitting diode," in *The Pacific Rim Conference on Lasers and Electro-Optics,* 1999.

[5] D. T. Reid, M. Padgett, C. McGowan, W. E. Sleat and W. Sibbett, "Light-emitting diodes as measurement devices for femtosecond laser pulses," *Optics Letters,* 1997.

[6] N. C. Hooten, "Characterization Of The Two-Photon Absorption Carrier Generation," Vanderbilt University, Nashville, Tennessee, 2011.

[7] T. F. C. a. J. F. Weller, "Picosecond Optical Autocorrelation Experiments," *Applied Physics Letters*, vol. 48, no. 7, pp. 460-462, 1985.

[8] E. W. VanStryland, H. Vanherzeele, M. A. Woodall, M. J. Soileau, A. L. Smirl, S. Guha and T. F. Boggess, "Two photon absorption, nonlinear refraction, and optical limiting in semiconductors," *Optical Engineering,* vol. 24, no. 4, pp. 613-621, 1985.

[9] F. Laughton, J. H. Marsh and A. Kean, "Very sensitive two-photon absorption GaAs/AlGaAs waveguide detector for an autocorrelator," *Electronics Letters*, vol. 28, no. 17, pp. 1663-1665, 1992.

[10] H. K. Tsang, L. Y. Chan, J. B. D. Soole, H. LeBlanc, M. A. Koza and R. Bhat, "High sensitivity autocorrelation using two-photon absorption in InGaAsP waveguides," *Electronics Letters,* vol. 31, no. 20, pp. 1773-1775, 1995.

[11] A. Zavriyev, E. Dupont, P. B. Corkum, H. C. Liu and Z. Biglov, "Direct autocorrelation measurements of mid-infraredpicosecond pulses by quantum-well devices," *Optics Letters,* vol. 20, no. 18, pp. 1886-1888, 1995.

[12] V. Nathan, A. H. Guenther and S. S. Mitra, "Review of multiphoton absorption in crystalline solides," *Optical Society of America B,* vol. 2, no. 2, pp. 294-315, 1985.

[13] J. Faist, F. Capasso, C. Sirtori, D. L. Sivco, A. L. Hutchinson and S. N. G. Chu, "Measurement of the intersubband scattering rate in semiconductor quantum wells by excited state differential absorption spectroscopy," *Applied Physics Letters,* vol. 63, no. 10, pp. 1354-1356, 1993.

[14] Y. Takagi, T. Kobayashi, K. Yoshihara and S. Imamura, "Multiple- and single-shot autocorrelator based on two-photon conductivity in semiconductors," *Optics Letters,* vol. 17, no. 9, pp. 658-660, 1992.

[15] "Interferometric Autocorrelation," 2008. [Online]. Available: http://www.swampoptics.com/assets/tutorials-autocorrelation-interferometric-2015.pdf. [Accessed 20 October 2016].

[16] V. S. Dneprovskiĭ and S. M. Ok, "Role of absorption by nonequilibrium carriers in determination of two-photon absorption coefficient of CdSe and GaAs crystals," *Kvantovaya Elektron,* vol. 6, no. 3, pp. 298-300, 1976.

[17] H. C. C. Jr., D. D. Sell and K. W. Wecht, "Concentration dependence of the absorption coefficient for n− and p−type GaAs between 1.3 and 1.6 eV," *Journal of Applied Physics,* no. 46, pp. 250-256, 1975.

[18] P. D. Olszak, C. M. Cirloganu, S. Webster, L. A. Padilha, S. Guha, L. P. Gonzalez, S. Krishnamurthy, D. J. Hagan and E. W. V. Stryland, "Spectral and temperature dependence of two-photon and free-carrier absorption in InSb," *Physics Review B,* vol. 82, no. 23, 2010.

[19] S. Krishnamurthy, Z. G. Yu, L. P. Gonzalez and S. Guha, "Temperature- and wavelength-dependent two-photon and free-carrier absorption in GaAs, InP, GaInAs, and InAsP," *Journal Of Applied Physics,* vol. 109, 2011.

[20] S. Krishnamurthy, A. Sher and A. B. Chen, "Below band-gap optical absorption in semiconductor alloys," *Journal of Applied Physics,* vol. 88, no. 1, pp. 260-264, 2000.

[21] J. F. O'Hara, J. M. O. Zide, A. C. Gossard, A. J. Taylor and R. D. Averitt, "Enhanced terahertz detection via ErAs:GaAs nanoisland superlattices," *Applied Physics Letters,* vol. 88, p. 251119, 2006.

[22] "The Coherent Artifact in Modern Pulse," 2015. [Online]. Available: http://www.swampoptics.com/assets/tutorials-coherent-artifact-2015.pdf. [Accessed 20 October 2016].

[23] I. Gradshteyn and I. Ryzhik, Table of Integrals, Series, and Products, London: Academic Press, 1965.

[24] L. Barry, P. Bollond, J. Dudley, J. Harvey and R. Leonhardt, "Autocorrelation of ultrashort pulses at 1.5um based on nonlinear response of silicon photodiodes," *Electronics Letters*, vol. 32, pp. 1922-1923, 1996.

APPENDICES

This appendix details the foundational concepts of traditional second harmonic generation (SHG) autocorrelators, and is intended to provide a background for readers unfamiliar with these concepts.

A.1 Mathematical Foundations and Necessity of the Technique

Optical signals have been measured by photodiodes for many decades. These devices operate on a very simple principle: the signal generated by the device is directly proportional to the intensity of light incident on the device. This relationship is represented by the following equation:

$$S(t) \sim I(t). \tag{16}$$

However, Equation 1 is based on the fundamental assumption that an instantaneous change in intensity will result in an instantaneous change in signal, regardless of the time duration over which this change occurs. This is not true when dealing with sub-picosecond pulses. The response time of the photodiode is often on the order of microseconds, and the absolute fastest response of the amplifier would be in the nanosecond range. Therefore, the pulse occurs in far less time than the minimum resolution of the detection system, and the event cannot be measured directly.

Measuring fast optical pulses requires a more creative approach that leverages the utility of nonlinearity. The pulse is split using a beam splitter. Both copies of the pulse are focused at the same point in the SHG (nonlinear) crystal, but they do not arrive at the same time. One of the pulses is sent directly to the crystal, while the other is directed through a variable-length path before arriving at the same focus point. This basic setup is illustrated in *Figure 34*.

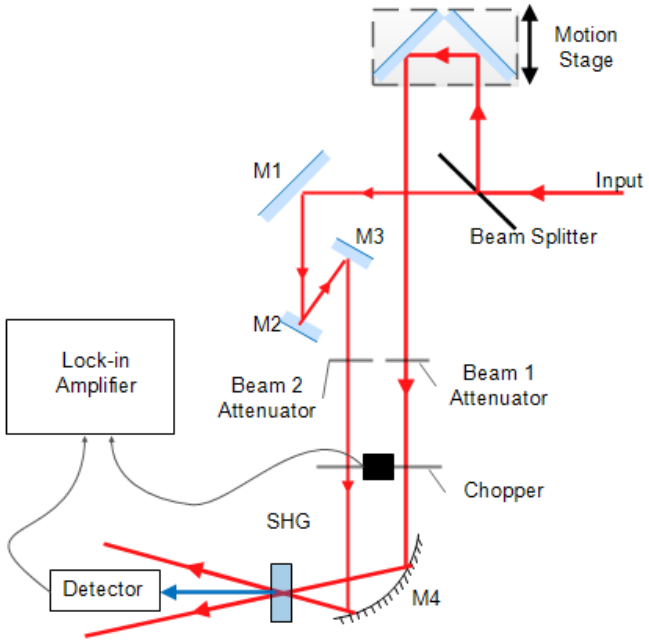

Figure 34: Intensity autocorrelation setup.

The total field at the SHG crystal is given by:

$$\mathrm{E}_{sig}(t) = E(t) + E(t-\tau). \tag{17}$$

This results in the second harmonic field:

$$\mathrm{E}^2_{sig}(t) = E^2(t) + 2E(t)E(t-\tau) + E^2(t-\tau). \tag{18}$$

The k-vectors of the cross term $E(t)E(t-\tau)$ cancel, while the $E^2(t)$ and $E^2(t-\tau)$ terms remain unaffected. This allows only the cross term to reach the detector, as illustrated in Figure 35.

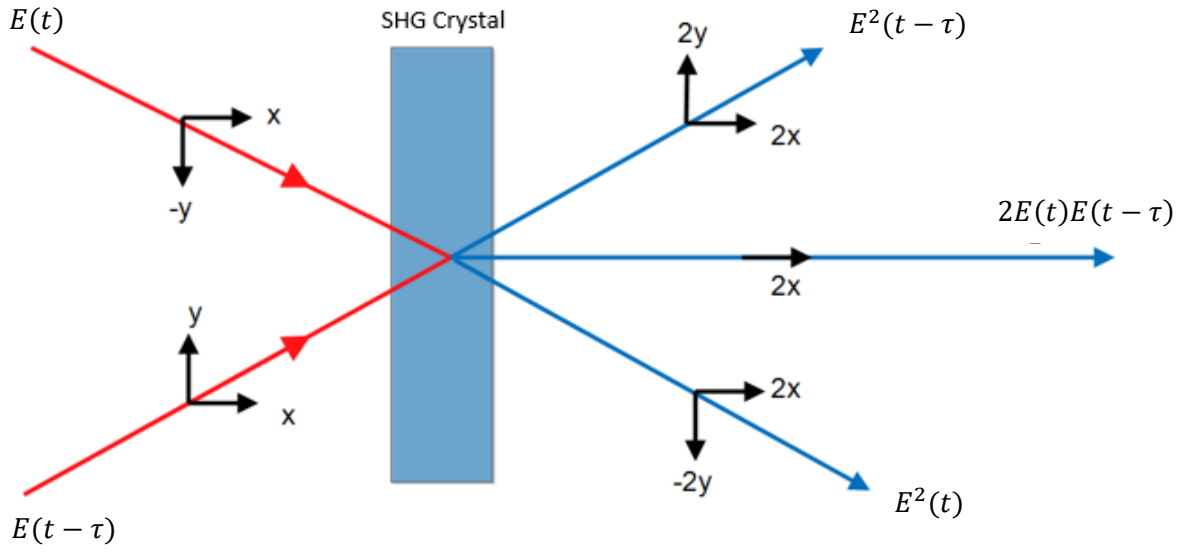

Figure 35: Direction of propagation through SHG crystal

The intensity of the field that reaches the detector is given by

$$I_{det}(t) = E_{sig}^2(t) = \{2E(t)E(t-\tau)\}^2 = 4I(t)I(t-\tau). \quad (19)$$

The detector and amplifier have a very slow response compared to the optical pulses. Both pulses will therefore finish hitting the detector long before an electrical response is observed. In this case, the current/voltage measured by the detector will represent the *total* number of carriers generated by both pulses. This is the physical equivalent of an integral in time according to the following expression:

$$A_c(\tau) = \beta \int_{-\infty}^{\infty} I_{det}(t)dt = \beta \int_{-\infty}^{\infty} I(t)I(t-\tau)dt. \quad (20)$$

Where the factor of four has been rolled into the term β, which is a measure of the strength of the nonlinearity in the crystal. This analysis highlights several important points. First, a nonlinear response is absolutely necessary for autocorrelation to be possible. Without the ability to square the fields, the cross-term multiplication would not happen, and the autocorrelation function would not be attainable. It is also important to observe that extra signal components exist which never

reach the detector. These components would not make a FWHM value determination impossible, and would in fact add information to the autocorrelation trace. This is sometimes utilized in interferometric autocorrelators, which send both beams through the SHG crystal collinearly to allow these signal components to reach the detector. However, this setup was not used in this work, and it is not analyzed here. Finally, it should be noted that the autocorrelation function cannot be obtained from one single pulse, since each pulse only provides one value of τ. Therefore, a scan of many delays using many pulses must be used to construct the complete profile for $A_c(\tau)$.

A.2 Measurement of Gaussian Pulses

For Gaussian pulses, the pulse intensity is given by:

$$I(t) = I_0 \exp\left(-\frac{t^2}{2\sigma^2}\right). \tag{21}$$

Where I_0 is the peak intensity of the pulse and σ is related to the FWHM value by the equation

$$FWHM = 2\sqrt{2ln(2)}\sigma. \tag{22}$$

Inserting Equation 21 into the standard autocorrelation formula gives

$$\begin{aligned} A_{Gauss}(\tau) &= \beta \int_{-\infty}^{\infty} I_0^2 exp\left(-\frac{t^2}{2\sigma^2}\right) \exp\left(-\frac{(t-\tau)^2}{2\sigma^2}\right) dt \\ &= \beta \int_{-\infty}^{\infty} I_0^2 \exp\left(\frac{-2t^2 + 2t\tau}{2\sigma^2}\right) \exp\left(-\frac{\tau^2}{2\sigma^2}\right) dt. \end{aligned} \tag{23}$$

Solutions for equations in the form of Equation 23 are given by [23]. This gives the following result:

$$A_{Gauss}(\tau) = \beta I_0^2 \sigma\sqrt{\pi}\exp\left(-\frac{\tau^2}{4\sigma^2}\right). \quad (24)$$

It should be noted that this result is still in the form of a Gaussian curve. However, the denominator in the exponential is different. It is instructive to put the result into the same form as the original Gaussian pulse:

$$A_{Gauss}(\tau) = \beta I_0^2 \sigma\sqrt{\pi}\exp\left(-\frac{\tau^2}{2\sigma'^2}\right). \quad (25)$$

Where $\sigma' = \sqrt{2}\sigma$. Since the result is still in Gaussian form, the FWHM value is still given by the same formula:

$$FWHM_{Autocorrelation} = 2\sqrt{2ln(2)}\sigma' = 2\sqrt{2ln(2)}\sqrt{2}\sigma. \quad (26)$$

Comparison to Equation 25 shows that the only difference between the FWHM value of the pulse and the FWHM value of the autocorrelation is the factor of $\sqrt{2}$, so

$$FWHM_{Autocorrelation} = \sqrt{2}FWHM_{Pulse}. \quad (27)$$

Therefore, the FWHM value of the original pulse can be obtained by dividing the FWHM value of the autocorrelation trace by $\sqrt{2}$. It should also be noted that this convenient relationship would not exist without nonlinearity. This nonlinearity allows the multiplication of intensity signals to be performed where the signals would normally be summed at the detector. Stronger nonlinearities will produce signals which are easier to read.

VITA

Ethan John Abele

Candidate for the Degree of

Master of Science

Thesis: MEASUREMENT AND ZERO-DELAY FINDING TECHNIQUES FOR ULTRASHORT OPTICAL PULSES USING LIGHT-EMITTING DIODES AS DETECTORS

Major Field: Electrical and Computer Engineering

Biographical:

Education:

Completed the requirements for the Master of Science in Electrical and Computer Engineering at Oklahoma State University, Stillwater, Oklahoma in December, 2016.

Completed the requirements for the Bachelor of Science in Electrical and Computer Engineering at Oklahoma State University, Stillwater, Oklahoma in 2014.

Teaching Experience:

Summer 2016	Introduction to Electrical Science (ECEN 2613), Oklahoma State University, Teaching Assistant
Spring 2016	Electromagnetic Fields (ECEN 3616), Oklahoma State University, Teach Assistant
Spring 2016	Introduction to Electrical Science (ECEN 2613), Oklahoma State University, Teaching Assistant
Fall 2014	Electromagnetic Fields (ECEN 3616), Oklahoma State University, Teaching Assistant

Publications:

Zhang, Y. et al. “Independently tunable dual-band perfect absorber based on graphene at mid-infrared frequencies”, Sci. Rep. 5, 18463; doi: 10.1038/srep18463 (2015)